10-20-2022

Enriched Dietary Saturated Fatty Acids Induce Trained Immunity via Ceramide Production that Enhances Severity of Endotoxemia and Clearance of Infection

Amy L. Seufert
Portland State University

James W. Hickman
Portland State University

Ste K. Traxler
Portland State University

Rachael M. Peterson
Portland State University

Trent A. Waugh
Portland State University

Citation Details

Seufert, A. L., Hickman, J. W., Traxler, S. K., Peterson, R. M., Waugh, T. A., Lashley, S. J., ... & Napier, B. A. (2022). Enriched dietary saturated fatty acids induce trained immunity via ceramide production that enhances severity of endotoxemia and clearance of infection. Elife, 11, e76744.

Enriched dietary saturated fatty acids induce trained immunity via ceramide production that enhances severity of endotoxemia and clearance of infection

Seufert AL[1], Hickman JW[1], Traxler SK[1], Peterson RM[1], Waugh TA[1], Lashley SJ[2], Shulzhenko N[3], Napier RJ[2,4], and Napier BA[1,*]

Author Affiliations: [1]Department of Biology and Center for Life in Extreme Environments, Portland State University, Portland, OR, 97201, [2]VA Portland Health Care System, Portland, OR, 97239, [3]Department of Biomedical Sciences, Oregon State University, Corvallis, OR, [4]Department of Molecular Microbiology and Immunology, Oregon Health & Science University, Portland, OR, 97239, United States.

*Corresponding Author: Dr. Brooke A Napier

Robertson Life Sciences Building

6th Floor Rm 6N087

Portland, OR 97201

E-mail address: brnapier@pdx.edu

Abstract

Trained immunity is an innate immune memory response that is induced by primary microbial or sterile stimuli that sensitizes monocytes and macrophages to a secondary pathogenic challenge, reprogramming the host response to infection and inflammatory disease. Nutritional components, such as dietary fatty acids, can act as inflammatory stimuli, but it is unknown if they can act as the primary stimuli in the context of innate immune memory. Here we find mice fed a diet enriched exclusively in saturated fatty acids (SFAs; ketogenic diet; KD) confer a hyper-inflammatory response to systemic lipopolysaccharide (LPS) and increased mortality, independent of diet-induced microbiome and glycemic modulation. We find KD mediates the composition of the hematopoietic stem cell (HSC) compartment, and macrophages derived from the bone marrow of mice fed KD do not have altered baseline inflammation, but enhanced responses to a secondary inflammatory challenge. Lipidomics identified enhanced free palmitic acid (PA) and PA-associated lipids in KD-fed mice serum. We found pre-treatment with physiologically relevant concentrations of PA alone reprograms macrophages to induce a hyper-inflammatory response to secondary challenge with LPS. This response was found to be dependent on the synthesis of ceramide, and reversible when treated with a ceramide synthase inhibitor. *In vivo*, we found systemic PA confers enhanced inflammation and mortality during an acute inflammatory response to systemic LPS, and this phenotype was not reversible for up to 7 days post-PA-exposure. While PA-treatment is harmful for endotoxemia outcome, we find PA exposure enhanced clearance of *Candida albicans* in *Rag1*$^{-/-}$ mice. Further, we show that oleic acid (OA), a mono-unsaturated FA that depletes intracellular ceramide, reverses the PA-induced hyper-inflammatory response shown in macrophages treated with LPS, and reduces severity and mortality of LPS endotoxin stimulation, highlighting the plasticity of SFA-dependent enhanced endotoxemia severity *in vivo.* These are the first data to implicate enriched dietary SFAs, and specifically PA, in the induction of long-lived innate immune memory that is detrimental during an acute inflammatory response, but beneficial for clearance of pathogens.

Introduction

Historically, immune memory has been defined as a trait limited to the adaptive immune system, however it is now well established that innate immune cells have the capacity for metabolic, epigenetic, and functional reprogramming that leads to long-lasting increases in host resistance to infection (*1-4*). Specifically, trained

immunity is an adaptation of innate host defense in vertebrates and invertebrates that results from exposure to a primary inflammatory stimulus and leads to a faster and greater response to a secondary challenge. Unlike adaptive memory responses, trained immunity does not require genome rearrangements, B and T lymphocytes, and receptors that recognize specific antigens (*1-4*). Further, trained immunity has been documented in organisms that lack canonical adaptive immune responses, such as plants and invertebrates, suggesting this is a primitive immune memory system that is conserved throughout vertebrates and invertebrates (*5*).

The Bacillus Calmette-Guérin (BCG) vaccine and yeast β-glucans are canonical inducers of trained immunity in humans and stimulate long-lasting metabolic and epigenetic reprogramming of myeloid-lineage cells resulting in hyperresponsiveness upon restimulation with heterologous or homologous inflammatory stimuli. This innate immune memory has been shown to be heritable (*6*) and can last up to months in humans and mice (*7*) and, thus, likely evolved to provide non-specific protection from secondary infections. Most recently, it was described that countries with higher rates of BCG vaccine at birth had fewer coronavirus disease 2019 (COVID-19) cases (*8*) making this immunological phenomenon extremely relevant. Importantly, it is easily ascertained that inflammatory hyperresponsiveness could be deleterious in the context of diseases where more inflammation can lead to greater pathology (ex: acute septic shock, autoimmune disorders, and allergies). Thus, trained immunity can be regarded as a double-edged sword – providing increased resistance to tissue-specific infection but exacerbating diseases exacerbated by systemic inflammation. Consequently, identifying novel inducers of trained immunity will provide clinically relevant insight into harnessing innate immune cells to attain long-term therapeutic benefits in a range of infections and inflammatory diseases.

Typically, the primary inflammatory stimulus that initiates trained immunity are danger- or pathogen-associated molecular patterns (DAMPs; PAMPs); however, recent publications have shown that β-glucan found in mushrooms, baker's and brewer's yeast, wheat and oats, and unknown components of bovine milk can induce trained innate immune memory in monocytes *in vitro* (*9, 10*). Our data reported here contribute to the growing evidence supporting the multifaceted immunoregulatory role of certain dietary constituents.

Currently, Westernized nations are increasingly dependent on diets enriched in saturated fatty acids (SFAs) (*11-13*), which have been shown to mimic PAMP effects on inflammatory cells, regulate innate immune cell function and alter outcomes of inflammatory disease and infection (*14-17*). Specifically, we have shown the

Western diet (WD), a diet enriched in sucrose and SFAs, correlates with increased disease severity and mortality in response to systemic LPS, independent of the diet-dependent microbiota, demonstrating the possibility that the dietary components of this diet may be driving the hyperresponsiveness to LPS (*18*). Currently, it is unknown if enriched dietary SFAs alone mediate trained immunity.

Our work presented herein identifies a ketogenic diet (KD) enriched exclusively in SFAs, and not sucrose, confers an increased systemic response to LPS independent of diet-associated microbiome, ketosis, or glycolytic regulation during disease, and alters inflammatory capacity and composition of the hematopoietic compartment. While others have shown that the WD induces trained immunity in atherosclerotic mice ($Ldrl^{-/-}$), we are the first to show that trained immunity, including its hallmark long-term persistence, can be induced in wild-type (WT) mice with exposure to enriched SFAs alone (*19*). A lipidomic analysis of blood fat composition after KD exposure revealed a significant increase of free palmitic acid (PA; C16:0) and fatty acid complexes containing PA. PA is known to act synergistically with LPS to enhance intracellular ceramide levels and proinflammatory cytokine expression in macrophages, however it is currently unknown if ceramide, a bioactive sphingolipid, specifically mediates a heightened inflammatory response to LPS following pre-exposure to PA (*20, 21*). Here we find macrophages pre-treated with physiologically relevant concentrations of PA followed by a secondary exposure to LPS leads to enhanced proinflammatory cytokine expression and release, which was reversible with the inhibition of ceramide.

We find that both short- and long-term exposure to PA, the predominant SFA found in high-fat diets, enhances systemic response to microbial ligands in mice even after a 7-day rest period from PA exposure. Thus, our data suggest exposure to PA leads to a long-lasting innate immune memory response *in vivo* (*7*). Importantly, trained immunity is induced when a primary inflammatory stimulus changes transcription of inflammatory genes, the immune status returns to basal levels, and challenge with a secondary stimulus enhances transcription of inflammatory cytokines at much higher levels than those observed during the primary challenge (*22*). While the dynamics of an initial inflammatory event induced by PA *in vivo* are not defined in this paper, we show that basal levels of *Tnf*, *Il6*, *Il1b* and *Il10* in the blood of mice pre-exposed to PA were comparable to control mice immediately prior to endotoxin challenge, indicating that mice were not in a primed state prior to disease. This suggests that the hyper-inflammation and poor disease outcome we show in PA-exposed mice is not due to priming, but a trained immune response.

The dual nature of trained immunity is also a hallmark feature of the phenomenon, in that non-specific innate immune memory can be either beneficial or detrimental depending on the disease context. The majority of research has demonstrated the protective role of trained immunity against a variety of infections, such as with BCG vaccination and B-glucan stimulation (*3, 23*). Our work is unique because we focus on the detrimental role that trained immunity has on disease characterized by inflammatory dysregulation, however we also highlight the beneficial nature of this novel phenotype by showing that when mice lacking adaptive immunity (*Rag1*$^{-/-}$) are pre-exposed to systemic PA, they exhibit enhanced clearance of kidney fungal burden compared to control mice.

We further identify a novel role of SFA-dependent intracellular ceramide required for the enhanced systemic response to microbial ligands, and show intervention with oleic acid, a mono-unsaturated fatty acid that depletes PA-dependent ceramide, can reverse these phenotypes in macrophages and *in vivo*. Our data presented here highlight the dynamic plasticity of dietary intervention on inflammatory disease outcomes. These data are consistent with the current knowledge that SFAs and ceramide are immunomodulatory molecules, and build on these by highlighting a previously unidentified role of PA in driving long-lived trained immunity.

Results

Diets enriched in saturated fatty acids increase endotoxemia severity and mortality

To examine the immune effects of chronic exposure to diets enriched in SFAs on lipopolysaccharide (LPS)-induced endotoxemia, we fed age matched (6 – 8 wk), female BALB/c mice either a WD (enriched in SFAs and sucrose), a ketogenic diet (KD; enriched in SFAs and low-carbohydrate), or standard chow (SC; low in SFAs and sucrose), for 2 weeks (wk) (Supplementary File 1). We defined 2 wk of feeding as chronic exposure, because this is correlated with WD- or KD-dependent microbiome changes, and confers metaflammation in WD mice (*18*), sustained altered blood glucose levels in WD mice (Fig 1 - figure supplement 1A), and elevated levels of ketones in the urine and blood in KD mice (Fig 1 - figure supplement 1 B-C). We then induced endotoxemia by a single intraperitoneal (i.p.) injection of LPS. We measured hypothermia as a measure of disease severity and survival to determine outcome (*18, 24, 25*). WD- and KD-fed mice showed significant and prolonged hypothermia, starting at 10 hours (h) post-injection (p.i.), compared to the SC-fed mice (Fig 1A). In

accordance with these findings, WD- and KD-fed mice displayed 100% mortality by 26 h p.i. compared to 100% survival of SC-fed mice (Fig 1B). Hypoglycemia is a known driver of endotoxemia, and each of these diets has varying levels of sugars and carbohydrates (Supplementary File 1) (*26, 27*). However, mice in all diet groups displayed similar levels of LPS-induced hypoglycemia during disease (Fig 1 - figure supplement 1D), indicating that potential effects of diet on blood glucose were not a driver of enhanced disease severity.

Considering mice fed KD experience a shift towards nutritional ketosis, we wanted to understand if our phenotype was dependent on nutritional ketosis. 1,3-butanediol is a compound that induces ketosis by enhancing levels of the ketone β-hydroxybutyrate in the blood (*28*). Age matched (6 – 8 wk), female BALB/c mice were fed for 2 wk with KD, SC supplemented with saccharine and 1,3-butanediol (SC + BD) or SC-fed with the saccharine vehicle solution (SC + Veh). BD supplementation was sufficient to increase blood ketones (Fig 1 - figure supplement 1 C). We next injected LPS i.p. and found KD-fed mice showed significantly greater hypothermia, and increased mortality, compared to SC + BD and SC + Veh (Fig 1 - figure supplement 1 E-F). Though short-lived, when compared to SC + Veh, the SC + BD mice did confer an increase in hypothermia, suggesting that nutritional ketosis may play a minor role in KD-dependent susceptibility to endotoxemia (Fig 1 - figure supplement 1 E-F). Together these data suggest that diets enriched in SFAs promote enhanced acute endotoxemia severity and this is independent of diet-dependent hypoglycemic shock or nutritional ketosis.

Diets enriched in SFAs induce a hyper-inflammatory response to LPS and increased immunoparalysis

Endotoxemia mortality results exclusively from a systemic inflammatory response characterized by an acute increase in circulating inflammatory cytokine levels (ex: TNF, IL-6, and IL-1β) from splenocytes and myeloid derived innate immune cells (*29-32*). Additionally, pre-treatment of myeloid-derived cells with dietary SFAs has been shown to enhance inflammatory pathways in response to microbial ligands (*33, 34*). Considering this, we hypothesized that exposure to enriched systemic dietary SFAs in WD- and KD-fed mice would enhance the inflammatory response to systemic LPS during the acute inflammatory response. Five-hours p.i., age matched (6 – 8 wk), female BALB/c mice fed all diets showed induction of *Tnf, Il6*, and *Il1b* expression in the blood (Fig 1C-E). However, at 5 h p.i., WD- and KD-fed mice experienced significantly higher expression of *Tnf* and *Il6* in the blood, compared with SC-fed mice, and WD-fed mice also showed significantly higher *Il1b* expression (Fig 1C-E), indicating that diets enriched in SFAs are associated with a hyper-inflammatory response to LPS.

Importantly, septic patients often present with two immune phases: an initial amplification of inflammation, followed-by or concurrent-with an induction of immune suppression (immunoparalysis), that can be measured by a systemic increase in the anti-inflammatory cytokine IL-10 (*35, 36*). Further, in septic patients, a high IL-10:TNF ratio equates with the clinical immunoparalytic phase and correlates with poorer sepsis outcomes (*37, 38*). Interestingly, we found there was significantly increased *Il10* expression in WD- and KD-fed mice, compared to SC-fed mice (Fig 1F), and WD- and KD-fed mice had significantly higher *Il10:Tnf* ratios at 10-20 h and 15-20 h, respectively, compared to SC-fed mice (Fig 1G). These data conclude that mice exposed to diets enriched in SFAs show an initial hyper-inflammatory response to LPS, followed by an increased immunoparalytic phenotype, which correlates with enhanced disease severity, similar to what is seen in the clinic.

Diets enriched in SFAs drive enhanced responses to systemic LPS independent of diet-associated microbiome

We have previously shown that WD-fed mice experience increased endotoxemia severity and mortality, independent of diet-associated microbiome (*18*). In order to confirm the increases in disease severity that correlated with KD were also independent of KD-associated microbiome changes, we used a germ free (GF) mouse model. 19-23 wk old female and 14 – 23 wk old male and female GF C57BL/6 mice were fed SC, WD, and KD for 2 wk followed by injection with 50 mg/kg of LPS, our previously established LD_{50} in GF C57BL/6 mice (*18*). As we saw in the conventional mice, at 10 h p.i. WD- and KD-fed GF mice showed enhanced hypothermia and mortality, compared to SC-fed GF mice (Fig 1H, I). These data show that, similar to WD-fed mice, the KD-associated increase in endotoxemia severity and mortality is independent of diet-associated microbiome.

Our previous studies (Fig 1A-G) in conventional mice were carried out in 6 – 8 wk female mice on a BALB/c background. Importantly, genetic background and age differences can have large effects on LPS treatment outcome. The GF mice used in this study (Fig 1H-N) were on a C57BL/6 background, between the ages of 14 – 23 wk. Thus, we confirmed WD- and KD-fed conventional C57BL/6 mice aged 20 – 21 wk old show enhanced disease severity and mortality in an LPS-induced endotoxemia model (4.5 mg/kg), compared to mice fed SC, similar to what is seen in younger BALB/c mice (Fig 1 - figure supplement 1 G-H).

Additionally, to confirm that the hyper-inflammatory response to systemic LPS was independent of the WD- and KD-dependent microbiome, we measured systemic inflammation during endotoxemia via the expression of *Tnf*, *Il6*, and *Il1b* in the blood at 0-10 h p.i. We found, WD- and KD-fed GF mice displayed enhanced expression of *Tnf* and *Il1b* at 5-10 h, and significantly enhanced expression of *il-6* at 5 h, compared to SC-fed GF mice (Fig 1J-L). Interestingly, *Il10* expression and the *Il10:Tnf* ratio were not significantly different throughout all diets, suggesting the SFA-dependent enhanced immunoparalytic phenotype is dependent on the diet-associated microbiomes in WD- and KD-fed mice (Fig 1M-N). These data demonstrate that the early hyper-inflammatory response, but not the late immunoparalytic response, to LPS associated with enriched dietary SFAs is independent of the diet-dependent microbiota.

A diet enriched exclusively in SFAs induces trained immunity

Thus far we find feeding diets enriched in SFAs (WD and KD) leads to enhanced expression of inflammatory cytokines in the blood after treatment with systemic LPS, suggesting that the SFAs may be inducing an innate immune memory response that leads to a hyper-inflammatory response to secondary challenge. Specifically, trained immunity is an innate immune memory response characterized by reprogramming of myeloid cells by a primary inflammatory stimulus, that then respond more robustly to secondary inflammatory challenge. Trained immunity has been shown to mediate cell sub-types within the hematopoietic stem cell (HSC) compartment that give rise to “trained” myeloid progeny for weeks to years (*39*). A previous study in *Ldlr*$^{-/-}$ mice has shown 4 wk of WD feeding significantly enhances multipotent progenitors (MPPs) and granulocyte and monocyte precursors (GMPs) and skews development of GMPs toward a monocyte lineage that are primed to respond with a hyper-inflammatory response to LPS (*19*). Currently, it is unknown if diets enriched in SFAs fed to WT mice, can induce changes within the HSC compartment or long-lasting trained immunity.

In order to determine the impact of dietary SFAs on bone marrow reprogramming *in vivo*, we next evaluated HSCs and progenitor cells via FACS from age-matched (6 – 8 wk) female WT BALB/c mice fed SC, WD and KD for 2 wk. Using previously published panels for analyzing HSC populations in the bone marrow (*23, 40, 41*), we collected bone marrow and measured relative proportions of long-term HSCs (LT-HSCs; CD201^{+}CD27^{+}CD150^{+}CD48^{-}), short-term HSCs (ST-HSCs; CD201^{+}CD27^{+}CD150^{+}CD48^{+}), and multipotent progenitors (MPPs; CD201^{+}CD27^{+}CD150^{-}CD48^{+}) (Fig 2A, B). Strikingly, we find that KD-fed mice showed

significantly enhanced ST- and LT-HSCs, and MPPs compared to SC-fed mice (Fig 2C). Unlike previously reported in *Ldlr*$^{-/-}$ mice, there was no significant change in ST-HSCs, LT-HSCs, or MPPs within WD-fed WT mice (Fig 2C). Further, we did not see a significant increase in MPP3s for WD-fed mice, as previously published for Ldlr$^{-/-}$ mice (*19*), or KD-fed mice; however, this may be due to the difference in genetic backgrounds, or length of diet administration (Fig 2 - figure supplement 1 A). These data are the first to show that the KD, a diet solely enriched in SFAs, alters hematopoiesis by enhancing expansion and differentiation of HSCs, similar to previously described inducers of trained immunity.

Further, it is unknown if enriched dietary SFAs lead to long-lasting functional reprogramming associated with trained immunity, that leads to a hyper-inflammatory response. Thus, we fed age-matched (6 – 8 wk) female BALB/c mice SC, WD, or KD for 2 wk, isolated bone marrow, differentiated into BMDMs for 7 days, and analyzed baseline inflammation and response to LPS. We found that untreated BMDMs isolated from mice fed SC and WD showed no significant differences in TNF or IL-6, and those from KD-fed mice showed a modest increase only in IL-6 compared to BMDMs from SC-fed mice (Fig 2 - figure supplement 1B). However, when BMDMs were stimulated with LPS for 24 h *ex vivo*, BMDMs from WD- and KD-fed mice showed significantly higher secretion of TNF, and only those from KD-fed mice showed significantly enhanced IL-6 secretion (Fig 2D-E). These data show that diets enriched in SFAs are inducing long-lasting inflammatory reprogramming of myeloid cells *in vivo,* and that reprogramming takes place within the bone marrow.

Importantly, monocytes and splenocytes are necessary for induction of systemic inflammatory cytokines during endotoxemia (*31, 32*). Thus, we wanted to assess if enriched dietary SFA induces *in vivo* reprogramming of monocytes and splenocytes, leading to an enhanced response to LPS *ex vivo.* First, we fed age-matched (6 – 8 wk) female BALB/c mice SC, WD, or KD for 2 wk, isolated bone marrow monocytes (BMMs) via magnetic negative selection using bone marrow extracted from femurs and tibias, and determined baseline expression of inflammatory cytokines. We found that prior to *ex vivo* LPS stimulation, BMMs isolated from mice fed SC, WD, or KD showed no significant difference in *Tnf* expression, and *Il6* expression was significantly decreased in BMMs from KD-fed mice (Fig 2 - figure supplement 1 C). However, when BMMs were stimulated with LPS for 2 h *ex vivo*, those from KD-fed mice showed significantly higher expression of *Tnf* and *Il6*, while those from WD-fed mice exhibited no significance in expression compared to SC-fed mice (Fig 2 - figure supplement 1 D). Similarly, we isolated splenocytes from SC-, WD-, and KD-fed mice and found no

difference between homeostatic inflammation of splenocytes between diets, but a significantly enhanced expression of *Tnf* in the splenocytes of KD-fed mice, and not WD-fed mice, challenged with LPS (2 h) compared to splenocytes from SC-fed mice (Fig 2 - figure supplement 1 E-F).

These data show the KD stimulates expansion of HSC populations, and skew differentiation of myeloid progenitors that then give rise to macrophages with enhanced inflammatory potency (Fig 2A-E; Fig 2 - figure supplement 2). Further, these data suggest that BMDMs, BMMs, and splenocytes from WD- and KD-fed mice are not more inflammatory at homeostasis; however, when challenged with LPS, KD feeding confers a hyper-inflammatory response. Together, our results suggest the KD, a diet that is comprised of 90.5% SFAs, leads to reprogramming of the HSC compartment and long-lasting trained immunity.

Palmitic acid (PA) and PA-associated fatty acids are enriched in the blood of KD-fed mice

It is known that the SFAs consumed in the diet determine the SFA profiles in the blood (*42-44*) and that these SFAs have the potential to be immunomodulatory. Thus, we next wanted to identify target SFAs enriched in the blood of mice fed a diet exclusively enriched in SFAs that may be altering the systemic inflammatory response to LPS. Considering that the KD is enriched in SFAs and not sucrose, and that KD-fed mice showed distinct HSC alterations and LPS-induced hyper-inflammation in BMDMs, BMMs, and splenocytes treated *ex vivo*, the subsequent studies were performed exclusively on KD-fed mice. We used mass spectrometry lipidomics to create diet-dependent profiles of circulating fatty acids in SC- and KD-fed mice (*45*). Age matched (6 – 8 wk), female BALB/c mice were fed SC or KD for 2 wk, then serum samples were collected and analyzed using qualitative tandem liquid chromatography quadrupole time of flight mass spectrometry (LC-QToF MS/MS). We used principal component analysis (PCA) to visualize how samples within each data set clustered together according to diet, and how those clusters varied relative to one another in abundance levels of free fatty acids (FFA), triacylglycerols (TAG), and phosphatidylcholines (PC). For all three groups of FAs, individual mice grouped with members of the same diet represented by a 95% confidence ellipse with no overlap between SC- and KD-fed groups (Fig 3A-C). These data indicate that 2 wk of KD feeding is sufficient to alter circulating FFAs, TAGs, and PCs, and that SC- and KD-fed mice display unique lipid blood profiles. Similarly, the relative abundance of sphingolipids (SG) in SC- and KD-fed mice displayed unique diet-dependent profiles with no overlapping clusters, and abundance of specific SGs were significantly higher in the serum of KD-fed

mice compared to SC-fed mice (Fig 3 - figure supplement 1 A-B). Though the independent role of each FFA, TAG, PC, and SG species has not been clinically defined, each are classes of lipids that when accumulated is associated with metabolic diseases, which have been shown to enhance susceptibility to sepsis and exacerbate inflammatory disease (*16, 46-48*).

Importantly, we identified a significant increase in multiple circulating FFAs within the KD-fed mice, compared to the SC-fed mice, many of which were SFAs (Fig 3D). Interestingly, in KD-fed mice we found a significant increase in free palmitic acid (PA; C16:0), an immunomodulatory SFA that is found naturally in animal fats, vegetable oils, and human breast milk (*49*), and is 8-fold enriched in KD (Fig 3D, Supplementary File 1). Additionally, PA-containing TAGs and PCs were significantly elevated in KD-fed mice serum, compared to SC-fed mice (Fig 3 - figure supplement 1 C-D). These data indicate that KD feeding not only enhances levels of freely circulating PA, but also enhances the frequency PA is incorporated into other lipid species in the blood.

Palmitic acid enhances macrophage inflammatory response to lipopolysaccharide

Many groups have shown that PA alone induces a modest, but highly reproducible increase in the expression and release of inflammatory cytokines in macrophages and monocytes (*14, 50*). However, it remains unknown if PA can act as a primary inflammatory stimulus to induce a hyper-inflammatory response to a secondary heterologous stimulus in primary cells. Thus, we next wanted to determine if pre-exposure to physiologically relevant concentrations of PA altered the macrophage response to a secondary challenge with LPS. Current literature indicates a wide range of serum PA levels, between 0.3 – 4.1 mM, reflect a high-fat diet in humans (*51*) (*52-55*). We aimed to use a physiologically relevant concentration of PA reflecting a human host for our *in vitro* studies, thus we treated primary bone marrow-derived macrophages (BMDMs) with and without 1 mM of PA containing 2% bovine serum albumin (BSA) for 12 h, removed the media, subsequently treated with LPS (10 ng/mL) for an additional 24 h, and measured expression and release of TNF, IL-6, and IL-1β. Importantly, the BSA dissolved in the media used for PA treatment solutions was endotoxin- and FA-free to ensure aberrant TLR signaling would not occur via BSA-contamination, and fresh PA was conjugated to BSA-containing media immediately prior to use. We found that BMDMs pre-treated with PA (1 mM) for 12 h expressed significantly higher levels of *Tnf* and *Il6* in response to secondary treatment with LPS, compared to naïve BMDMs (Fig 3E,

F). *Il1b* expression was significantly lower in cells pre-treated with PA (Fig 3G), however, secretion of TNF, IL-6 and IL-1β were all enhanced in BMDMs pre-treated with PA (1 mM) for 12 h and challenged with LPS (Fig 3H-J). We found a similar enhanced *Il6* and *Tnf* expression in response to LPS in BMDMs treated with PA (1 mM) for twice the length of exposure (24 h), and *Il-1b* expression was decreased (Fig 3 - figure supplement 2 A-C).

Further, we pre-treated BMDMs with a concentration of PA that reflects the lower range of physiologically relevant serum levels and found 0.5 mM of PA induced significantly higher expression of *Tnf, Il6* and *Il1b* after 12 h challenge with LPS, however only *Tnf* and *Il6* were significantly enhanced after 24 h LPS treatment, compared to naive BMDMs treated with LPS (Fig 3 - figure supplement 2 D-I).

Importantly, PA-treatment can induce apoptosis and pyroptosis in various cell types (*56-59*), however we found only an average of 3.4% and 4.4% of cell death after a 12 h or 24 h incubation, respectively, with PA (1 mM) and subsequent 24 h of LPS treatment or control media (Fig 3 - figure supplement 3 A-B). These data demonstrate PA pre-treatment of macrophages induces a hyper-inflammatory response to LPS independent of cell death, suggesting PA is sensitizing macrophages to secondary inflammatory challenge.

Thus, we conclude that both 12 and 24 h pre-treatments with 0.5 mM or 1 mM of PA conjugated to 2% BSA are sufficient to induce reprogramming of macrophages and alter the response to stimulation with a heterologous ligand. Additionally, these data demonstrate that even serum concentrations of PA that are at the lower end of the spectrum for humans consuming a high-fat diet pose a risk for inflammatory dysfunction.

Diverting ceramide synthesis inhibits the PA-dependent hyper-inflammatory response to LPS in macrophages

PA treatment of various cell types diverts cellular metabolism toward the synthesis of the toxic metabolic byproducts: diacylglycerols (DAGs) and ceramide (*60*). PA-induced ceramide synthesis has specifically been demonstrated to enhance inflammation (*20, 21, 33, 61*). Considering this, we wanted to determine the role of enhanced macrophage ceramide production in driving PA-induced hyper-inflammatory response to LPS. Thus, we treated BMDMs simultaneously with PA (0.5 mM) and a ceramide synthase inhibitor Fumonisin B1 (FB1; 10 μM), for 12 h, removed the media, subsequently treated with LPS (10 ng/mL) for an additional 24 h, and measured release of TNF, IL-6, and IL-1β. We found that BMDMs pre-treated simultaneously with PA and FB1 for 12 h expressed significantly lower levels of TNF, IL-6, and IL-1β secretion in response to LPS, compared to

BMDMs pre-treated with only PA (Fig 3K-M). We conclude that ceramide synthesis induced by PA is required for the macrophage hyper-inflammatory response to secondary challenge with LPS.

Palmitic acid is sufficient to increase endotoxemia severity and systemic hyper-inflammation

Considering the drastic effect of PA on macrophage response to secondary challenge with LPS, we next wanted to understand if exposure to PA alone is sufficient to induce a hyper-inflammatory response during endotoxemia *in vivo*. We answered this question using age-matched (6 – 8 wk) female BALB/c mice fed SC for 2 wk, by mimicking systemic PA levels found in serum of humans on high-fat diet via a single i.p. injection of ethyl palmitate (750 mM), and then after 12 h, challenging with LPS i.p. (*62*). Similar to previous publications, we find that a 750 mM i.p. injection of ethyl palmitate enhances free PA levels in the serum to 173 – 425 μM compared to Veh-treated mice with 110 – 250 μM (Fig 4 - figure supplement 1 A). Important to note, free PA is only transiently enhanced by systemic application, and is quickly (<1 h) taken up by peripheral tissues; thus, our detected free serum levels are most likely an underestimation of transient systemic PA (*63-65*).

Interestingly, after LPS challenge, PA-treated mice experienced increased disease severity as indicated by their significant decline in temperature compared to Veh mice (Fig 4A). Similar to WD- and KD-fed mice, PA-treated mice also exhibited enhanced mortality, compared to Veh mice (Fig 4B). Importantly, mice injected with PA for shorter time periods (0, 3, and 6 h) and then challenged with LPS did not exhibit increased disease severity or poor survival outcome (Fig 4 - figure supplement 1 B-C), concluding that a 12 h pre-treatment with PA is required for an increase in disease severity.

Next, we measured systemic inflammatory status during disease and found similar to KD-fed mice, the 12 h PA-pre-treated mice showed significantly enhanced expression of *Tnf* (5 h and 10 h) and *Il6* (5 h) post-LPS challenge, compared to Veh control (Fig 4C, D). Expression of *Il-1b* trended upward, but was not significantly up-regulated in 12 h PA-pre-treated mice, compared to Veh-treated mice (Fig 4E). Importantly, as a control we looked at LPS-induced hypoglycemia in PA-treated mice, and 12 h pre-treatment with PA did not alter LPS-induced hypoglycemia (Fig 4 - figure supplement 1 D), indicating that diet-dependent hypoglycemic shock was not a driver of endotoxemia severity in PA-treated mice. Thus, exposure to PA to mimic systemic levels found in humans eating high-fat diets is sufficient to drive enhanced inflammation and disease severity in mice stimulated with endotoxin, and this effect is dependent on length of PA exposure.

PA induces long-lived hyperresponsiveness to LPS and enhanced clearance of fungal infection

Our data show that pre-treatment with systemic PA alone enhances endotoxemia severity *in vivo*, and enhances inflammatory responses of macrophages to a secondary and heterologous stimulus *in vitro*. This form of regulation resembles trained immunity; however, it remains unclear if PA is inducing trained immunity *in vivo*. We first evaluated the basal level expression of *Tnf, Il6,* and *Il1b* in mice treated with 750 mM of PA or Veh i.p. for 12 h, before stimulation with LPS. Interestingly, we did not see significant differences in *Tnf, Il6,* or *Il1b* expression at 12 h of exposure with PA (Fig 4F), which suggests that circulating immune cells of these mice are not in a primed state at these time points prior to LPS injection. These data suggest PA induces trained immunity, and not priming, however the time point of initial inflammation induced by PA remains unknown.

As mentioned previously, canonical inducers of trained immunity (e.g., BCG or β-glucan) induce long-lived enhanced innate immune responses to secondary inflammatory stimuli (*23, 66*). Thus, we hypothesized that exposure to a PA bolus would enhance disease severity and mortality in mice, and that this phenotype would persist even after mice were rested from PA injections for 1 wk. We injected age matched (6 – 8 wk), female BALB/c mice fed SC with a vehicle solution (Veh→SC) or PA (750 mM; PA→SC) i.p. once a day for 9 d and then rested the mice for 1 wk. When challenged with systemic LPS, PA→SC showed an increase in disease severity and mortality compared to Veh→SC mice (Fig 4G, H), indicating that PA alone can induce long-lived trained immunity that increases susceptibility to inflammatory disease. Importantly, the difference between Veh→SC and PA→SC survival was not significant (Fig 4H), suggesting PA is not the sole driver of the enhanced mortality we see in KD.

Lastly, the most commonly studied models for inducing trained immunity are immunization with BCG or stimulation with β-glucan, and they have been shown to protect mice from systemic *Candida albicans* infection via lymphocyte-independent immunological reprogramming that leads to decreased kidney fungal burden (*2*). Therefore, we next tested if PA treatment induces lymphocyte-independent clearance of *C. albicans* infection. For these experiments, *Rag1* knockout (*Rag1*$^{-/-}$) mice were treated with a vehicle or PA solution for 12 h and subsequently infected intravenously (i.v.) with $2x10^6$ *C. albicans*. In accordance with canonical trained immunity models, mice treated with PA for 12 h showed a significant decrease in kidney fungal burden

compared to Veh mice, 24 h post-infection (Fig 4I). These are the first data to suggest PA enhances innate immune clearance of *C. albicans in vivo*.

Oleic acid reverses enhanced disease severity in WD- and KD-fed mice.

We have reported here that diversion of ceramide synthesis reverses the PA-dependent hyper-inflammatory response to LPS in macrophages *in vitro* (Fig. 3K-M). Interestingly, oleic acid (C18:1) is a mono-unsaturated fatty acid naturally found in animal fats and vegetable oils, and in the presence of PA, diverts lipid metabolism away from ceramide production (*60, 67*). Considering OA and PA are the most prevalent fatty acids found in the human diet and in human serum (*60*), we wanted to test if OA diversion of ceramide synthesis could reverse the PA-dependent hyper-inflammatory response to LPS in macrophages. Thus, we treated BMDMs with OA (0.2 mM), PA (0.5 mM), or OA and PA together for 12 h and then with LPS. We found that macrophages simultaneously pre-treated with PA and OA produced significantly lower levels of TNF, IL-6, and IL-1β following subsequent LPS exposure, compared to BMDMs pre-treated with only PA prior to LPS stimulation (Fig 5A-C). These data reveal OA-dependent depletion of intracellular ceramides neutralizes the PA-dependent hyper-inflammatory response to LPS in macrophages.

Considering this, we next wanted to know if i.p. injections of OA in KD-fed mice would mitigate enriched dietary SFA-associated disease severity and mortality. Thus, we fed age-matched (6 – 8 wk) female BALB/c mice SC or KD for 2 wk and injected them i.p. with 300 mM oleic acid or Veh once per day for the final 3 d of feeding. We then injected LPS i.p. and measured hypothermia and survival. Veh-injected KD-fed mice showed significant and prolonged hypothermia starting at 8 h p.i., compared to SC-fed mice (Fig 5D). In accordance with these findings, KD-fed mice displayed significantly enhanced mortality by 24 h p.i., compared to 100% survival of SC-fed mice (Fig 5E). Strikingly, for KD-fed mice injected with 300 mM OA prior to LPS treatment, there was minimal temperature loss comparable to SC-fed mice, and 100% survival (Fig 5D, E). Together, these data show systemic OA can abrogate KD-dependent hypothermia and survival defect in response to LPS in mice fed diets enriched solely in SFA, and highlight the fascinating plasticity of dietary fatty acid reprogramming of innate immune cell populations and disease dynamics.

Discussion

In this study we showed that mice fed diets enriched in SFA exhibit hyper-inflammation during endotoxemia and poorer outcomes, compared with mice fed a standard low-SFA diet, independent of the diet-associated microbiome, ketosis, and the impact of each diet on LPS-induced hypoglycemia (Fig 1; Fig 1 - figure supplement 1). Strikingly, we found that before LPS treatment, healthy mice fed a diet solely enriched in SFAs (Ketogenic diet; KD) displayed significant expansion of HSCs, including MPPs, and harbored BMDMs, BM monocytes, and splenocytes that were not inherently more inflamed, but when challenged with LPS exhibited increased production of inflammatory cytokines (Fig 2; Fig 2 - figure supplement 1, Fig 2 - figure supplement 2). Since (1) we did not confer the hyper-inflammatory phenotype in BMDMs, BMMs, and splenocytes with WD, but only from KD-fed mice, and (2) the KD is only enriched in SFAs and contains no sucrose, allowing us to ask questions specifically about SFAs, we chose to focus on the KD for the remainder of the study.

Considering the immunogenic properties of some dietary SFAs enriched in the KD, and that excess dietary SFAs are found circulating throughout the blood and peripheral tissues, we used lipidomics to identify dietary SFAs that may be directly reprogramming innate immune cells to respond more intensely to secondary inflammatory stimuli. Our study identified enriched palmitic acid (C16:0; PA) and PA-associated fatty acids in the blood of KD-fed mice (Fig 3; Fig 3 - figure supplement 1). And, when we treated macrophages with physiologically relevant concentrations of PA, we found that PA alone induces a hyper-inflammatory response to secondary challenge with LPS (Fig 3; Fig 3 - figure supplement 2). This enhanced production of inflammatory cytokines in response to secondary heterologous stimuli has been shown in previous models of innate immune memory, specifically trained immunity (*4, 19, 68*). Further, our data suggests PA induces trained immunity by showing that circulating inflammatory levels in PA-injected mice were not upregulated or in a primed state prior to LPS stimulation *in vivo* (Fig 4F), and PA-associated enhanced endotoxemia severity and mortality is still shown in mice rested for 7 days post-PA exposure (Fig 4G-H). Importantly, we have not fully defined the initial inflammatory response to PA in our model, thus our data only suggests trained immunity is induced by PA exposure. However, we do find that PA- exacerbates the acute phase of endotoxin challenge and correlates with increased mortality, but also enhances resistance to infection independent of mature lymphocytes (Fig 4). Together, our data concludes PA exposure can lead to hallmark phenotypes associated with canonical trained immunity models *in vitro* and *in vivo*.

Interestingly, the *in vivo* blood expression of cytokines for KD-fed mice following endotoxin challenge is mild in comparison to the cytokine secretion we show for BM monocytes, splenocytes, and BMDMs isolated from KD-fed mice treated with LPS *ex vivo* (Fig 1; Fig 2; Fig S2). The media used for culturing and treating BM monocytes and splenocytes *ex vivo* with LPS contained a high-glucose concentration (4.5 g/L; 25 mM). However, high-glucose media does not alter TNF, IL-6, or IL-1β secretion, or mitochondrial metabolic activity, in WT BMDMs treated with LPS following 7 d of differentiation in high-glucose media (*69*). Additionally, in these studies, metabolic adaptation likely takes place within 48 h for BMDMs cultured in high glucose media (*69*); thus, we suggest it is unlikely that high-glucose contributed to the significant augmentation of LPS-induced TNF and IL-6 secretion for BMDMs from KD-fed mice compared to controls, following 7 d of differentiation in high-glucose media prior to LPS challenge. However, further studies on the metabolic flexibility of the SC- and KD-BMDMs will be required to answer this question directly.

Additionally, we have previously shown that WD-induced weight gain does not correlate with enhanced endotoxemia severity and mortality in conventional mice (*18*). This is important to address because of the "obesity paradox" that describes the diversity in sepsis severity and mortality exhibited within the obese patient population, with some studies showing that obesity may even be protective in certain disease contexts (*70*). Humans on an animal-based KD that contains 76% fat with 30% SFA content, and 10% carbohydrates, experience ketosis within 1-2 wk characterized by a 3- to 4-fold elevation in blood BHB levels, and exhibit greater energy expenditure and weight loss compared to humans on a low-fat, plant-based diet that contains 10% fat and 75% carbohydrates (*71*). Likewise, KD-fed mice do not gain weight, but show enhanced energy expenditure after 5 wk of diet administration, and a trend toward weight loss during 9 wk of diet exposure, compared to mice fed a standard chow diet (*72*). Thus, neither weight gain or the obesity paradox are confounding features for the data we present here showing that both KD and dietary PA mediate innate immune memory *in vivo* during endotoxemia.

Further, the metabolism of dietary SFAs is a key element of immune system function, and metabolic intermediates enhanced by SFAs and PA alone, such as ceramide, serve as signaling lipids in diseases of inflammation (*73*). Mechanistically, we show that inhibiting ceramide synthesis or diverting metabolism away from ceramide synthesis using OA protects macrophages from PA-induced trained immunity, suggesting that dietary intervention may help regulate inflammatory dysregulation during disease (Fig 5). And, to complement

our *in vitro* mechanistic findings we show that 3 single i.p. injections of OA prior to endotoxin stimulation protects KD-fed mice from enhanced disease severity and mortality (Fig 5).

Our findings align with the growing body of evidence indicating that trained immunity is a double-edged sword, where the phenomenon can be beneficial for resistance to infection, but detrimental in the context of diseases exacerbated by systemic inflammation (*74*). Specifically, we show that PA-induced memory is beneficial in that it promotes clearance of *C. albicans* infection in the kidneys of *Rag1*$^{-/-}$ mice (Fig 4I). In stark contrast, PA-induced memory is detrimental in the context of endotoxemia, a disease driven by organ damage due to acute hyper-inflammation (*75-79*) (Fig 4G, H). Further, it is known that trained immunity is a key feature of BCG vaccination, which has been shown to enhance resistance to infections, and is a possible mechanism that drives increased resistance to severe COVID-19 in the BCG vaccinated population (*7, 80*). Thus, future research in understanding the plasticity of the SFA- and PA-regulated immune memory responses, enhanced pathogen clearance, and the mechanisms that drive this phenomenon, will be of interest to the larger medical community.

Mechanistically, it is appreciated that PA is not acting as a ligand for the pattern recognition receptor (PRR) TLR4, however the presence of TLR4 (independent of TLR4 signaling capability) is required for PA-dependent inflammation (*14*). Our data and others contribute to the growing evidence that PA is inducing cell intrinsic stress through alterations in metabolism. The crosstalk between glycolytic and oxidative metabolism, and epigenetics, is crucial for trained immunity in human monocytes, and metabolic intermediates of the TCA cycle directly modify histone methylation patterns associated with proinflammatory cytokines upregulated in trained immunity (*4, 81, 82*). While ceramides are known to modify histone acetylation and DNA methylation patterns (*83*), the interplay between ceramide metabolism and epigenetics within innate immune cells has not been explored. Though we have shown that PA-dependent ceramide production leads to innate immune memory, the impact of these alterations on the epigenome remains unknown. Therefore, the influence of ceramide metabolism on epigenetics will be important to consider in future trained immunity studies where PA serves as the primary stimulus.

Interestingly, we find here that immunoparalysis, which is associated with a prolonged septic response and is enhanced in patients with poorer outcomes, is greater in mice fed diets enriched in SFAs (Fig 1) (*37, 38*). However, we found that this SFA-dependent enhanced immunoparalysis is abrogated in germ-free mice,

suggesting, for the first time, that the microbial species within the SFA-fed mice may be regulating the late immunoparalytic phase of endotoxin shock. Considering the clinical correlation of immunoparalysis and increased sepsis mortality, it will be imperative to explore the identity of the SFA-dependent microbiome and the host/microbe mechanisms that drive sepsis-associated immunoparalysis.

Importantly, previous seminal studies concluded that mice treated with antibodies to the TNF receptor and challenged with systemic LPS increased survival from 0% to nearly 100%, suggesting that acute inflammation driven by TNF is responsible for endotoxemia-related mortality (*75, 76*). Further, it has been shown that TNF is required for acute renal failure (*77*), lung injury (*78*), and liver damage (*79*) during LPS challenge. These data show that acute inflammation, specifically the bioactivity of TNF, drives endotoxemia mortality and organ damage in conventional mice. It has also been shown that acute inflammation, specifically TNF production, is a driver of endotoxemia in GF mice (*84*). Thus, although our conventional mice show increased immunoparalysis, we suggest that early acute systemic inflammation is the driver of disease severity and mortality in both our conventional and GF endotoxemia mouse models; however, the data we present here is not sufficient to make this conclusion.

In conclusion, this unappreciated role of dietary SFAs, specifically PA, may provide insight into the long-lasting immune reprogramming associated with a high-SFA fed population, and lends insight into the complexity of nutritional immunoregulation. Considering the results in this study, we suggest the potential for SFAs such as PA to directly impact innate immune metabolism and epigenetics associated with inflammatory pathways. Thus, our findings are paramount not only for potential dietary interventions, but also treatment of inflammatory diseases exacerbated by metabolic dysfunction in humans.

Materials and Methods

Cell lines and reagents. RAW 264.7 macrophages (from ATCC), CASP-1KO BMDMs, BMDMs and BMMs were maintained in DMEM (Gibco) containing L-glutamine, sodium pyruvate, and high glucose supplemented with 10% heat-inactivated fetal bovine serum (FBS; GE Healthcare, SH3039603). BMDMs were also supplemented with 10% macrophage colony-stimulating factor (M-CSF; M-CSF-conditioned media was collected from NIH 3T3 cells expressing M-CSF, generously provided by Denise Monack at Stanford University).

Generation of BMDMs, BMMs, and splenocytes. Bone marrow-derived macrophages (BMDMs) and bone marrow-derived monocytes (BMMs) were harvested from the femurs and tibias of age-matched (6-8 wk) CO_2-euthanized female BALB/c mice or male and female C57BL/6J mice. BMDM media was supplemented with 10% macrophage colony-stimulating factor (M-CSF) for differentiation, cells were seeded at 5 x 10^6 in petri dishes and cultured for 6 days, collected with cold PBS, and frozen in 90% FBS and 10% DMSO in liquid nitrogen for later use. BMMs were isolated from BMDM fraction using EasySep™ Mouse Monocyte Isolation Kit (STEMCELL). Spleens were harvested from age-matched (6-8 wk) CO_2-euthanized female BALB/c mice, tissue was disrupted using the end of a syringe plunger on a 70 µm cell strainer and rinsed with FACS buffer (PBS + 2mM EDTA). Cells were subjected to red blood cell lysis with RBC lysing buffer (Sigma) followed by neutralization in FACS buffer.

Treatments. After thawing and culturing for 5 days, BMDMs were pelleted and resuspended in DMEM containing 5% FBS, 2% endotoxin- and fatty acid-free bovine serum albumin (BSA; Proliant Biologicals) and 10% M-CSF. Cells were seeded at 2.5 x 10^5 cells/well in 24-well tissue-culture plates, treated with EtOH (1.69%, or 0.83%) 10 ng/mL LPS (Ultrapure LPS, *E. coli* 0111:B4, Invivogen), 500 µM or 1 mM palmitic acid (Sigma-Aldrich, PHR1120), 10uM Fumonisin B1 (Sigma-Aldrich, F1147), or 200 µM oleic acid (Sigma-Aldrich, O7501). and incubated at 37°C and 5% CO_2 for 12 or 24 h. Next, cells were treated with an additional 10 ng/mL LPS, and incubated an additional 12 or 24 h. RAW 264.7 macrophages were thawed and cultured for 3-5 days, pelleted and resuspended in DMEM containing 5% FBS and 2% endotoxin- and fatty acid-free BSA, and treated identical to BMDM treatments. BMMs were seeded immediately after harvesting at 4 x 10^5 cells/well in 96-well V-bottom plates in DMEM containing 10% FBS, and treated with LPS for 2 or 24 h. Splenocytes were seeded immediately after harvesting at 1 x 10^5 cells/well in 96-well V-bottom plates in RPMI media with L-glutamine (Cytiva) containing 10% FBS, and treated with LPS for 2 or 24 h. BMDMs for *ex vivo* treatments were isolated as described above, plated at 2.5 x 10^5 cells/well in 24-well plates, and stimulated with 10 ng/mL LPS after 12 h of adherence. For all treatments, supernatant was removed for ELISA analysis, and cells were lysed with TRIzol (ThermoFisher), flash-frozen in liquid nitrogen, and stored at -80°C until qRT-PCR analysis. For all plates, all treatments were performed in triplicate.

Flow Cytometry. Modified panel using combined methods from Kaufmann et al., Nowlan et al., and Vasquez et al. Red blood cells were lysed in BM cells using RBC lysis buffer (Biolegend). BM cells (3 x 10^6 cells) were stained with viability stain Live/Dead Fixable Aqua (ThermoFisher) at the concentration of 1:200 for 30 minutes at 4°C. Next, cells were washed with FACS buffer (PBS supplemented with 0.5% BSA; Proliant Biologicals, fatty acid free), and incubated with anti-CD16/32 (clone 93, BioLegend) at a concentration of 1:100 in FACS buffer for 10 minutes at 4°C. The following antibodies were then used for staining HSCs, and MPPs: anti-Ter-110, anti-CD11b (clone M1/70), anti-CD5 (clone 53-7.3), anti-CD4 (clone RM4-5), anti-CD8a (clone 53-6.7), anti-CD45R (clone RA3-6B2), and anti-Ly6G/C (clone RB6-8C5), all biotin-conjugated (all BD Bioscience), were added at a concentration of 1:100 for 30 minutes at 4°C, and washed with FACS buffer. Streptavidin-APC-Cy7 (eBioscience), anti-CD150-eFluor450 (clone Q38-480, eBioscience), anti-CD48-PerCPeFluor710 (BD Bioscience), anti-Flt3-PE (clone A2F10.1, BD Bioscience), anti-CD34-PEDazzle 594 (clone HM34, BioLegend), anti-CD27-PE-Cy7 (eBioscience), and anti-CD201-APC (eBioscience) were added all at a concentration of 1:100 for 20 minutes at 4°C. All cells were then washed with FACS buffer before and after incubation in 1% paraformaldehyde for 30 minutes at 4°C. Cells were acquired on BD flow cytometer (FACSymphony A1 Cell Analyzer) with FACSDiva Software. Analyses were performed using FlowJo software v.10.1. The DownSample version 3.3.1 plugin was used to standardize events for each sample after populations were gated.

Lactate dehydrogenase (LDH) assays. BMDMs were cultured as stated above with culture media, PA, or ethanol in 96-well tissue-culture plates at a concentration of 5 x 10^4 cells/well and incubated for 12 hours. Cells were treated with PBS or 10 ng/mL LPS in a phenol-red-free Optimem media (ThermoFisher) and incubated an additional 12 or 24 h. Supernatants were collected at the specified time points with LDH release quantified with a CytoTox96 Non-Radioactive Cytotoxicity Assay (Promega). Cytotoxicity was measured per well as a percentage of max LDH release, with background media-only LDH release subtracted. For all plates, all treatments were performed in triplicate.

Measurement of cell viability. Cell viability was determined by 0.4% Trypan Blue dye exclusion test executed by a TC20 Automated Cell Counter (Bio-Rad).

Blood RNA extraction and real-time qPCR. Mice were treated with PBS or LPS, and at specified time points 10-20 µL of blood was collected from the tail vein, transferred into 50 µL of RNALater (ThermoFisher Scientific) and frozen at -80°C. RNA extractions were performed using RNeasy Mini Kit (Qiagen) and cDNA was synthesized from RNA samples using SuperScript III First-Strand synthesis system (Invitrogen). Gene specific primers were used to amplify transcripts using SsoAdvanced Universal SYBR Green Supermix (Bio-Rad). A complete list of all primers used, including the names and sequences, is supplied as Supplementary File 2.

Enzyme-linked immunosorbent assay (ELISA). TNF, IL-6, and IL-1β concentrations in mice serum were measured and analyzed using TNF, IL-6, and IL-1β Mouse ELISA Kits (ThermoFisher Scientific), according to the manufacturer's instructions. Absorbances were measured at a wavelength of 450 nm using a microplate reader (BioTek Synergy HTX). Values below the limit of detection (LOD) of the ELISA were imputed with LOD divided by 2 (LOD/2) values.

LPS-induced endotoxemia model. Age-matched (6 – 8 wk) female BALB/c mice were anesthetized with isoflurane and injected subcutaneously with ID transponders (Bio Medic Data Systems). 2 wk post diet change, and 1 wk post ID transponder injection, mice were stimulated with a single injection of 6-10 mg/kg LPS reconstituted in endotoxin-free LAL reagent water (Invivogen) and diluted in PBS for a total volume of 200 µL. Control mice received corresponding volumes of PBS. Progression of disease was monitored every 2 h after LPS injection for clinical signs of endotoxin shock based on weight, coat and eyes appearance, level of consciousness and locomotor activity. Age-matched (20 – 21 wk) female C57BL/6 mice were treated as described above, except for their LPS dose (4.5 mg/kg). Temperature was recorded using a DAS-8007 thermo-transponder wand (Bio Medic Data Systems). For PA injections, a solution of 750 mM ethyl palmitate (Millipore Sigma), 1.6% lecithin (Sigma-Aldrich) and 3.3% glycerol was made in endotoxin-free LAL reagent water (Lonza). The lecithin-glycerol-water solution was used as a vehicle, and mice were injected with 200 µL of the vehicle as a control, or ethyl palmitate solution to increase serum PA levels. For OA injections, a solution

of 300 mM OA (Sigma-Aldrich) was made using the same solution and vehicle described above. Mice were injected i.p. with 200 µL of the vehicle as a control, or OA solution, between 7 – 9 pm for 3 d prior to LPS exposure.

Mouse diets, glucose, and ketones. Six-week-old female mice were fed soft, irradiated chow (PicoLab Mouse Diet 20, product 5058) and allowed to acclimate to research facility undisturbed for one week. Chow was replaced by Western Diet (Envigo, TD.88137), Ketogenic Diet (Envigo, TD.180423), or Standard Chow (Envigo, TD.08485) and mice were fed *ad libitum* for two weeks before induction of endotoxemia. For Ketogenic Diet, food was changed daily. For Western Diet, food was changed every 72 hours. Ketones and blood glucose were measured weekly and immediately prior to LPS injections with blood collected from the tail vein using Blood Ketone & Glucose Testing Meter (Keto-Mojo), or with urine collected on ketone indicator strips (One Earth Health, Ketone Test Strips).

Statistics analysis. Mann Whitney, Mantel-Cox, and student's t-tests were carried out with GraphPad Prism 9.0 software.

Ethical approval of animal studies. All animal studies were performed in accordance with National Institutes of Health (NIH) guidelines, the Animal Welfare Act, and US federal law. All animal experiments were approved by the Oregon Health and Sciences University (OHSU) Department of Comparative Medicine or Oregon State University (OSU) Animal Program Office and were overseen by the Institutional Care and Use Committee (IACUC) under Protocol IDs #IP00002661 & IP00001903 at OHSU and #5091 at OSU. Conventional animals were housed in a centralized research animal facility certified by OHSU. Conventional 6-10 wk-aged female BALB/c mice (Jackson Laboratory 000651) were used for the endotoxemia model, and isolation of BMDMs, BMMs, and splenocytes. GF male and female C57BL/6 mice (Oregon State University; bred in house) between 14 and 23 wk old were used for the GF endotoxemia model. BALB/c *Rag1*$^{-/-}$ mice between 8 and 24 wk were infected i.v. with 2x10^{6} CFUs of *C. albicans* SC5314 (ATCC #MYA-2876) and kidney fungal burden was assessed 24 h post-infection. Kidneys were harvested 24 h post-infection and homogenized organs were plated in serial dilutions on Yeast Peptone Dextrose plates to assess fungal burden.

643

644 **Lipidomics PCA Analysis**

645 Mice on specialized diets were sacrificed at the indicated time points after PBS or LPS treatment with 300-
646 600µL of blood collected via cardiac puncture into heparinized tubes. Blood samples were centrifuged for 15
647 minutes at 2,500rpm at 4°C and serum was transferred to a new tube before storage at -80°C. Serum samples
648 were analyzed via LC-MS/MS. Lipidomic data sets were scaled using the *scale* function and principal
649 component analyses were performed using the *prcomp* function from the stats package in R Version 3.6.2.
650 Visualization of PCAs and biplots was performed with the *fviz_pca_ind* and *fviz_pca_biplot* functions from the
651 factoextra package and with the *ggplot2* package (*85, 86*). For each diet group, 95% confidence ellipses were
652 plotted around the group mean using the *coord.ellipse* function from the FactoMineR package (*87*). Heatmaps
653 were created using the *pheatmap* package (*88*).

654

655 **Acknowledgements**

656 We would like to thank Ajesh Saini, a student in the Napier Lab, for his contributions in carrying out the ELISA
657 data within this manuscript. This study was supported by National Institute of General Medical Sciences
658 (NIGMS) grant 5R35GM133804-02 to B.A.N.

659

660 **Figure Legends**

661 **Fig. 1 Diets enriched in SFAs lead to enhanced endotoxemia severity and altered systemic**
662 **inflammatory profiles, independent of diet-associated microbiome. (A-G)** Age-matched (6 – 8 wk) female
663 BALB/c mice were fed SC, WD, or KD for 2 wk and injected i.p. with 6 mg/kg of LPS. **(A)** Temperature loss and
664 **(B)** survival were monitored every 2 h. At indicated times 10 – 20 µL of blood was drawn via the tail vein, RNA
665 was collected, and samples were assessed for expression of **(C)** *Tnf,* **(D)** *Il6,* **(E)** *Il1b,* and **(F)** *Il10* via qRT-
666 PCR. **(G)** *Il10:Tnf* ratio was calculated for 5, 10, 15, and 20 hours p.i. with LPS. **(H-N)** Next, 19 – 23 wk old
667 female and 14 – 23 wk old male and female germ-free C57BL/6 mice were fed SC, WD, or KD for 2 wk and
668 injected i.p. with 50 mg/kg of LPS. **(H)** Temperature loss and **(I)** survival were monitored every 5 h p.i. **(J-N)** At
669 indicated times, 10-20 µL of blood was drawn via the tail vein, RNA was collected, and samples were
670 assessed for expression of **(J)** *Tnf,* **(K)** *Il6,* **(L)** *Il1b,* and **(M)** *Il10* via qRT-PCR. **(N)** *Il10:Tnf* ratio was calculated

for 5 and 10 h p.i. with LPS. For **A-G,** n = 5 per diet group, and data are representative of 1 experiment. For **H-N,** SC, n = 6; WD, n = 5, and KD, n = 9, and data are representative of 1 experiment. For **A, C-G, H,** and **J-N** a Mann Whitney test was used for pairwise comparisons. For **B** and **I** a log-rank Mantel-Cox test was used for survival curve comparison. For all panels, *p< 0.05; **p < 0.01; ***p< 0.001. For **C-E**, Φ symbols indicate WD significance and ∞ symbols indicate KD significance. Error bars shown mean ± SD.

Fig. 2 KD feeding alters HSC populations and BMDMs from KD-fed mice show a hyper-inflammatory response to LPS *ex vivo*. Bone marrow was extracted from the femurs and tibias of age-matched (6 – 8 wk) female BALB/c mice fed SC, WD, or KD for 2 wk. **(A)** FACS plots of total HSCs ($CD201^+CD27^+$) and **(B)** LT-HSCs, ST-HSCs, and MPPs from mice fed SC, WD, or KD for 2 wk. Quantification of **(C)** the total numbers of LT- and ST-HSCs, and MPPs in BM from mice fed SC, WD, or KD for 2 wk. Next, BMDMs were plated at 5x10^6 cells/mL, and differentiated for 7 d in media supplemented with M-CSF. Cells were split and plated in 24-well plates to adhere for 12 h, and treated with media (Ctrl) or LPS (24 h; 10 ng/mL). Supernatants were assessed via ELISA for **(D)** TNF and **(E)** IL-6 secretion at 24 h post-LPS treatment. IL-6 Ctrl supernatants were below the limit of detection; ND = no data. **(C)** a Mann Whitney test was used for pairwise comparisons. **(D, E)** For all plates, all treatments were performed in triplicate, and a student's t-test was used for statistical significance. *, p < 0.05; **, p < 0.01; ***, p < 0.001; ****, p < 0.0001. Error bars show the mean ± SD.

Fig. 3 KD alters lipid profiles and PA is mediating a hyper-inflammatory response to secondary challenge with LPS. Data points represent single animal samples and colors represent groups fed SC (grey) or KD (orange) diets for two weeks. A 95% confidence ellipse was constructed around the mean point of each group for **(A)** free fatty acids (FFA), **(B)** triglycerides (TAG), and **(C)** phosphatidylcholines (PC). **(D)** Heatmap analysis of free fatty acids in SC and KD mice. Components that are significantly different between the two groups are in bold. Below the heatmap is a comparison of palmitic acid 16:0 peak area detected by LC-MS/MS between SC and KD groups; AUC = area under the curve. Statistical significance is determined by unpaired two-tailed t-test between SC and KD groups with n=3 per group. Primary bone marrow-derived macrophages (BMDMs) were isolated from aged-matched (6 – 8 wk) C57BL/6 female and male mice. BMDMs were plated at $1x10^6$ cells/mL and treated with either ethanol (EtOH; media with 0.83% ethanol), media (Ctrl for LPS), or LPS

(10 ng/mL) for 12 h, or palmitic acid (PA stock diluted in 0.83% EtOH; 1 mM PA conjugated to 2% BSA) for 12 h, with and without a secondary challenge with LPS. After indicated time points, RNA was isolated and expression of **(E)** *Tnf*, **(F)** *Il6*, **(G)** *Il1b* was measured via qRT-PCR. BMDMs were plated at $1x10^6$ cells/mL and treated with either ethanol (EtOH; media with 0.83% ethanol), media (Naïve), or 1 mM PA for 12 h followed by PBS (control) or LPS (10 ng/mL). Supernatants were assessed via ELISA for **(H),** TNF, **(I)** IL-6, and **(J)** IL-1β secretion. Next, BMDMs were plated at $1x10^6$ cells/mL and treated with either media (Ctrl), LPS (10 ng/mL) for 24 h, palmitic acid (PA stock diluted in 0.83% EtOH; 0.5 mM PA conjugated to 2% BSA) for 12 h, Fumonisin B1 (FB1; 10 μM; diluted in 0.14% EtOH) or EtOH (0.97% to mimic simultaneous PA/FB1 treatment). Controls for all treatments are shown next to experimental groups treated additionally with LPS (10 ng/mL) for 24 h. Supernatants were assessed via ELISA for **(K),** TNF, **(L)** IL-6, and **(M)** IL-1β secretion. For all plates, all treatments were performed in triplicate. For all panels, a student's t-test was used for statistical significance. *, $p < 0.05$; **, $p < 0.01$; ***, $p < 0.001$; ****, $p < 0.0001$. Error bars show the mean ± SD.

Fig. 4 PA acts as a novel mediator of trained immunity by inducing a hyper-inflammatory response LPS-induced endotoxemia, and enhancing clearance of *Candida albicans* infection. Age-matched (6 – 8 wk) female BALB/c mice were fed SC for 2 wk and injected i.p. with ethyl palmitate (PA, 750 mM) or vehicle (Veh) solutions 12 h before i.p. LPS injections (10 mg/kg). **(A)** Temperature loss was monitored every 2 h as a measure of disease severity or **(B)** survival. At indicated times blood was collected via the tail vein, RNA was extracted, and samples were assessed for expression of **(C)** *Tnf,* **(D)** *Il6,* and **(E)** *Il1b* via qRT-PCR. **(F)** Blood was collected via the tail vein from Vehicle (Veh) and PA pre-treated (12 h PA) mice immediately prior to LPS injection and samples were assessed for expression of *Tnf, Il6, Il1b*, and *Il10* via qRT-PCR. Additionally, age-matched (6 – 8 wk) female BALB/c mice fed SC, injected i.p. with ethyl palmitate (PA, 750 mM) or vehicle (Veh) solutions every day for 9 days, and then rested for 7 d before i.p. LPS injections (10 mg/kg) **(G)** Temperature loss and **(H)** survival were monitored during endotoxemia. **(I)** Age-matched (8-9 wk) female *Rag1*$^{-/-}$ mice were injected i.p. with ethyl palmitate (PA, 750 mM) or vehicle (Veh) solutions 12 h before i.v. *C. albicans* infection. Fungal burden of kidneys from Vehicle (Veh) and PA pre-treated (12 h PA) mice 24 h after *C. albicans* infection. For **(A-F),** experiments were run 3 times and data are representative of 1 experiment, n=3 mice/group. For **(G, H),** experiments were run twice, and data are representative of 1 experiment. For

Veh→SC, n=3 mice and PA→SC, n=5 mice. For **(I),** experiments were run 3 times and data are representative of 1 experiment, n=6 mice/group. For **(A)**, **(C-E), (G)** and **(I),** a Mann Whitney test was used for pairwise comparisons. For **(B)** and **(H),** a log-rank Mantel-Cox test was used for survival curve comparison. For all panels, *, $p < 0.05$; **, $p < 0.01$; ***, $p < 0.001$; ****, $p < 0.0001$. Error bars shown mean ± SD.

Fig. 5 Oleic acid reverses PA-dependent hyper-inflammation in response to LPS *in vitro*, and PA-dependent enhanced endotoxemia disease severity *in vivo*. Primary bone marrow-derived macrophages (BMDMs) were isolated from aged-matched (6 – 8 wk) C57BL/6 female and male mice. BMDMs were plated at $1x10^6$ cells/mL and treated with either media (Ctrl), LPS (10 ng/mL) for 24 h, palmitic acid (PA stock diluted in 0.83% EtOH; 0.5 mM PA conjugated to 2% BSA) for 12 h, or oleic acid (OA; 200 μM; diluted in endotoxin-free water). Controls for all treatments are shown next to experimental groups treated additionally with LPS (10 ng/mL) for 24 h. Supernatants were assessed via ELISA for **(A)** TNF, **(B)** IL-6, and **(C)** IL-1β secretion. Age-matched (6 – 8 wk) female BALB/c mice were fed SC or KD for 2 wk and injected i.p. with 7 mg/kg LPS or. **(D)** Temperature loss and **(E)** survival were monitored every 2 h. For **(A-C)**, a student's t-test was used for statistical significance. For **(D),** a Mann Whitney test was used for pairwise comparisons. For **(E),** a log-rank Mantel-Cox test was used for survival curve comparison. For **(D, E),** experiments were run 3 times and data are representative of 1 experiment, n=5 mice/group. β symbols indicate KD+Veh vs KD+OA significance, and ∞ symbols indicate KD+Veh vs. SC+ Veh. For all panels, *, $p < 0.05$; **, $p < 0.01$; ***, $p < 0.001$; ****, $p < 0.0001$. Error bars shown mean ± SD.

Supplementary Figure Legends

Figure 1 Supplementary Figure 1. Increase in disease severity in KD mice is independent of ketosis. Age-matched (6 – 8 wk) female BALB/c mice were fed SC, WD, or KD for 2 wk. At 1 wk and 2 wk, **(A)** blood was collected via the tail vein to measure blood glucose levels using a glucose testing meter (Keto-Mojo) and **(B)** urine was collected on ketone indicator strips to measure levels of systemic acetoacetate (AcAc). Age-matched (6 – 8 wk) female BALB/c mice were fed SC supplemented with 1,3-butanediol (SC + BD) or with a saccharine vehicle solution as a control (SC + Veh), or KD for 2 wk. At 1 wk and 2 wk, **(C)** blood was collected via the tail vein to measure levels of systemic β-hydroxybutyrate (BHB) using a ketone testing meter (Keto-

Mojo). At 2 wk, SC-, WD-, and KD-fed mice were injected i.p. with LPS (6 mg/kg) and **(D)** 25 h p.i. blood glucose levels were measured as stated in **A**. **(E)** temperature loss and **(F)** survival were monitored every 2 h for mice treated as in **C** followed by i.p. injection with LPS (10 mg/kg). Age-matched (20-21 wk) female C57BL/6 mice were fed SC, WD, or KD for 2 wk followed by i.p. injection with LPS (4.5 mg/kg). **(G)** temperature loss and **(H)** survival were monitored every 2 h. For **(A, B, D)** all experiments were run 3 times and data are representative of 1 experiment, n = 5-8 mice/group. For **(C, E, F)** all experiments were run 3 times and data are representative of 1 experiment, n = 5-8 mice/group. For **(G, H)** data are representative of 1 experiment, n = 10 mice/group. For **(A-C, E, G)** a Mann-Whitney U test was used for pairwise comparisons. For **(F, H)** a log-rank Mantel-Cox test was used for survival curve comparison. For **(E)** β symbols indicate SC + Veh vs. SC + BD significance, ∞ symbols indicate SC + Veh vs. KD significance, and δ symbols indicate SC + BD vs. KD significance. For **(G)** ϕ symbols indicate SC vs. WD significance, and ∞ symbols indicate SC w. KD significance. For all panels, * $p < 0.05$; ** $p < 0.01$; *** $p < 0.001$; **** $p < 0.0001$. Error bars show mean ± SD.

Figure 2 Supplementary Figure 1. KD does not alter MPP differentiation or basal inflammation in BMDMs, and monocytes and splenocytes show a hyper-inflammatory response to LPS *ex vivo.* Age-matched (6 – 8 wk) conventional, wild-type, female BALB/c mice were fed SC, WD, or KD for 2 wk. Bone marrow was extracted from the femurs and tibias of mice, HSCs were isolated via FACS and **(A)** MPPs were quantified. BMDMs were plated at $5x10^6$ cells/mL, and differentiated for 7 d in media supplemented with M-CSF. Cells were split and plated in 24-well plates to adhere for 12 h, and treated with media (Ctrl) for 24 h. Supernatants were assessed via ELISA for **(B)** TNF and IL-6 secretion. Monocytes were isolated from the femurs and tibias of mice and plated at $2x10^6$ cells/mL. RNA was extracted from **(C)** untreated monocytes (0 h) or **(D)** monocytes with LPS (10 ng/mL) for 2 h. Expression of *Tnf* and *Il6* was analyzed via qRT-PCR. Splenocytes were isolated and plated at $1x10^6$ cells/mL. RNA was isolated from **(E)** untreated splenocytes (0 h) or **(F)** splenocytes treated with LPS (10 ng/mL) for 2 h. Expression of *Tnf* and *Il6* was analyzed via qRT-PCR. n = 3 mice/group in each representative experiment. A student's t-test was used for statistical significance. For all panels, * $p < 0.05$; ** $p < 0.01$; *** $p < 0.001$; **** $p < 0.0001$. Error bars show mean ± SD.

Figure 2 Supplementary Figure 2. Gating strategy for HSCs, related to Figures 2 and 4. Cells were gated in FSC-A against SSC-A. Doublets were excluded using FSC-A against FSC-H and subsequently SSC-A against SSC-H. Viable cells were gated and lineage-committed cells were excluded. Within the lineage-negative cells, the $CD201^{+}CD27^{+}$ population was gated. In a CD150 against CD48 plot, the $CD201^{+}CD27^{+}$ cells were divided into LT-HSC, ST-HSC, MPP, and the remaining $CD150^{-}CD48^{-}$ population. MPPs were characterized as MPP3 and MPP4 by their surface expression of CD34 and Flt3.

Figure 3 Supplementary Figure 1. Principal component analysis (PCA) and heatmap analysis of sphingolipid lipidomic data in mouse serum samples. (A) Data points represent single animal samples and colors represent groups fed SC (grey) or KD (orange) diets for two weeks and a 95% confidence ellipse was constructed around the mean point of each group. Heatmap analysis of **(B)** sphingolipids (SM), **(C)** triglycerides (TG), and **(D)** phosphatidylcholines (PC) in SC and KD groups. Lipid components containing 16:0 palmitic chains are highlighted in purple and components that are significantly different between the two groups are in bold. Statistical significance determined by unpaired two-tailed t-test between SC and KD groups. * $p < 0.05$; ** $p < 0.01$; *** $p < 0.001$; **** $p < 0.0001$. n=3 per group.

Figure 3 Supplementary Figure 2. Physiological levels of Palmitic Acid induce a hyper-inflammatory response to secondary challenge with LPS in macrophages. Primary bone marrow-derived macrophages (BMDMs) were isolated from age-matched (6 – 8 wk) female and male mice. **(A-C)** BMDMs were plated at $1x10^6$ cells/mL and treated with ethanol (EtOH; media with 1.69% ethanol), media (Ctrl for LPS), or palmitic acid (PA, 1 mM; diluted in 1.69% EtOH) for 12 h. Next, PA-treated cells were treated with LPS (10 ng/mL) for 24 h, and all other wells were given fresh media. **(D-I)** BMDMs were plated at $1x10^6$ cells/mL and treated with PA (0.5 mM; diluted in 1.69% EtOH) for 12 or 24 h. Next, PA-treated cells were treated with LPS (10 ng/mL) for 24 h, and all other wells were given fresh media. After indicated time points, RNA was isolated and expression of **A, D, G** *Tnf,* **B, E, H** *Il6*, and **C, F, I** *Il1b* was measured via qRT-PCR. For all plates treatments were performed in triplicate. For all panels, a student's t-test was used for statistical significance. * $p < 0.05$; ** $p < 0.01$; *** $p < 0.001$; **** $p < 0.0001$. Error bars show mean ± SD.

Figure 3 Supplementary Figure 3. Cytotoxicity as determined by LDH release from BMDMs pre-treated with PA followed by LPS stimulation. BMDMs from age-matched (6 – 8 wk) male and female C57BL/6 mice were plated in 96-well plates at $5x10^4$ cells/well and incubated for 12 h with PA (0.5 mM or 1 mM). Next, media was removed, and cells were treated with PBS for 10 ng/mL LPS in phenol-red-free Opti-MEM media and incubated for an additional 24 h. Supernatants were collected and LDH release was quantified using CytoTox96 Non-Radioactive Cytotoxicity Assay. **(A, B)** Cytotoxicity is shown as percentage of max LDH release. For all plates all treatments were performed in triplicate, and a student's t-test was used for statistical significance. * $p < 0.05$; ** $p < 0.01$; *** $p < 0.001$; **** $p < 0.0001$. Error bars show mean ± SD.

Figure 4 Supplementary Figure 1. Palmitic acid i.p. injections enhance serum PA concentrations and PA-induced trained immunity is time-dependent. Conventional wild-type, age-matched (6 – 8 wk), female BALB/c mice were fed SC for 2 wk and injected i.p. with ethyl palmitate (PA 750 mM in 1.6% lecithin and 3.3% glycerol in endotoxin-free LAL reagent water) or a vehicle solution (Veh, 1.6% lecithin and 3.3% glycerol in endotoxin-free LAL reagent water). **(A)** serum was collected via cardiac punctures from mice 2 h and 5 h p.i. Serum samples were analyzed for absolute PA concentrations using qualitative tandem liquid chromatography quadrupole time of flight mass spectrometry (LC-QToF MS/MS). At 0, 3, and 6 h after PA injection, endotoxemia was induced via a single i.p. injection of LPS (10 mg/kg). **(B)** Temperature loss and **(C)** survival were monitored every 2 h. **(D)** blood was collected via the tail vein to measure blood glucose levels at 0 and 20 h p.i. with LPS using a glucose testing meter (Keto-Mojo). For **(D)** a Mann Whitney test was used for pairwise comparisons. Data is representative of 1 experiment, n = 3-4 mice/group. * $p < 0.05$; ** $p < 0.01$; *** $p < 0.001$; **** $p < 0.0001$. Error bars show mean ± SD.

Supplemental File 1. Diet compositions (values represent percentage of total kcal)

Supplemental File 2. List of primers used in this study

Figure 1 – Source data 1. Data and statistics for graphs depicted in Figure 1 A-N

Figure 2 – Source data 1. Data and statistics for graphs depicted in Figure 2 A-E

Figure 3 – Source data 1. Data and statistics for graphs depicted in Figure 3 A-M

Figure 4 – Source data 1. Data and statistics for graphs depicted in Figure 4 A-I

Figure 5 – Source data 1. Data and statistics for graphs depicted in Figure 5 A-E

Figure 1 – Figure Supplement 1 – Source data 1. Data for graphs depicted in Figure 1 – Figure Supplement 1 A-H

Figure 2 – Figure Supplement 1 – Source data 1. Data for graphs depicted in Figure 3 – Figure Supplement 1 A-F

Figure 3 – Figure Supplement 2 – Source data 1. Data for graphs depicted in Figure 3 – Figure Supplement 2 A-D

Figure 3 – Figure Supplement 3 – Source data 1. Data for graphs depicted in Figure 3 – Figure Supplement 3 A-B

Figure 4 – Figure Supplement 1 – Source data 1. Data for graphs depicted in Figure 4 – Figure Supplement 1 A-D

References

1. M. G. Netea *et al.*, Defining trained immunity and its role in health and disease. *Nat Rev Immunol* **20**, 375-388 (2020).
2. J. Kleinnijenhuis *et al.*, Bacille Calmette-Guerin induces NOD2-dependent nonspecific protection from reinfection via epigenetic reprogramming of monocytes. *Proc Natl Acad Sci U S A* **109**, 17537-17542 (2012).
3. J. Quintin *et al.*, Candida albicans infection affords protection against reinfection via functional reprogramming of monocytes. *Cell Host Microbe* **12**, 223-232 (2012).
4. S. Saeed *et al.*, Epigenetic programming of monocyte-to-macrophage differentiation and trained innate immunity. *Science* **345**, 1251086 (2014).
5. H. Lanz-Mendoza, J. Contreras-Garduno, Innate immune memory in invertebrates: Concept and potential mechanisms. *Dev Comp Immunol* **127**, 104285 (2022).
6. N. Katzmarski *et al.*, Transmission of trained immunity and heterologous resistance to infections across generations. *Nat Immunol* **22**, 1382-1390 (2021).
7. M. G. Netea *et al.*, Trained immunity: A program of innate immune memory in health and disease. *Science* **352**, aaf1098 (2016).

8. C. Covian, A. Retamal-Diaz, S. M. Bueno, A. M. Kalergis, Could BCG Vaccination Induce Protective Trained Immunity for SARS-CoV-2? *Front Immunol* **11**, 970 (2020).

9. D. K. Meena *et al.*, Beta-glucan: an ideal immunostimulant in aquaculture (a review). *Fish Physiol Biochem* **39**, 431-457 (2013).

10. M. van Splunter *et al.*, Induction of Trained Innate Immunity in Human Monocytes by Bovine Milk and Milk-Derived Immunoglobulin G. *Nutrients* **10**, (2018).

11. B. A. Swinburn *et al.*, The global obesity pandemic: shaped by global drivers and local environments. *Lancet* **378**, 804-814 (2011).

12. B. M. Popkin, Global nutrition dynamics: the world is shifting rapidly toward a diet linked with noncommunicable diseases. *Am J Clin Nutr* **84**, 289-298 (2006).

13. A. Christ, E. Latz, The Western lifestyle has lasting effects on metaflammation. *Nat Rev Immunol* **19**, 267-268 (2019).

14. G. I. Lancaster *et al.*, Evidence that TLR4 Is Not a Receptor for Saturated Fatty Acids but Mediates Lipid-Induced Inflammation by Reprogramming Macrophage Metabolism. *Cell Metab* **27**, 1096-1110.e1095 (2018).

15. C. N. Lumeng, J. L. Bodzin, A. R. Saltiel, Obesity induces a phenotypic switch in adipose tissue macrophage polarization. *J Clin Invest* **117**, 175-184 (2007).

16. P. J. Meikle, S. A. Summers, Sphingolipids and phospholipids in insulin resistance and related metabolic disorders. *Nat Rev Endocrinol* **13**, 79-91 (2017).

17. A. W. B. Reyes *et al.*, Protection of palmitic acid treatment in RAW264.7 cells and BALB/c mice during Brucella abortus 544 infection. *Journal of Veterinary Science* **22**, (2021).

18. B. A. Napier *et al.*, Western diet regulates immune status and the response to LPS-driven sepsis independent of diet-associated microbiome. *Proc Natl Acad Sci U S A* **116**, 3688-3694 (2019).

19. A. Christ *et al.*, Western Diet Triggers NLRP3-Dependent Innate Immune Reprogramming. *Cell* **172**, 162-175.e114 (2018).

20. J. D. Schilling *et al.*, Palmitate and Lipopolysaccharide Trigger Synergistic Ceramide Production in Primary Macrophages. *Journal of Biological Chemistry* **288**, 2923-2932 (2013).

21. Y. Zhang *et al.*, Adipose Fatty Acid Binding Protein Promotes Saturated Fatty Acid-Induced Macrophage Cell Death through Enhancing Ceramide Production. *J Immunol* **198**, 798-807 (2017).
22. M. Divangahi *et al.*, Trained immunity, tolerance, priming and differentiation: distinct immunological processes. *Nat Immunol* **22**, 2-6 (2021).
23. E. Kaufmann *et al.*, BCG Educates Hematopoietic Stem Cells to Generate Protective Innate Immunity against Tuberculosis. *Cell* **172**, 176-190 e119 (2018).
24. B. A. Napier *et al.*, Complement pathway amplifies caspase-11-dependent cell death and endotoxin-induced sepsis severity. *J Exp Med*, (2016).
25. H. Saito, E. R. Sherwood, T. K. Varma, B. M. Evers, Effects of aging on mortality, hypothermia, and cytokine induction in mice with endotoxemia or sepsis. *Mech Ageing Dev* **124**, 1047-1058 (2003).
26. C. F. Raetzsch *et al.*, Lipopolysaccharide inhibition of glucose production through the Toll-like receptor-4, myeloid differentiation factor 88, and nuclear factor kappa b pathway. *Hepatology* **50**, 592-600 (2009).
27. J. P. Filkins, R. P. Cornell, Depression of hepatic gluconeogenesis and the hypoglycemia of endotoxin shock. *Am J Physiol* **227**, 778-781 (1974).
28. E. L. Goldberg *et al.*, Ketogenic diet activates protective γδ T cell responses against influenza virus infection. *Sci Immunol* **4**, (2019).
29. A. J. Lewis, C. W. Seymour, M. R. Rosengart, Current Murine Models of Sepsis. *Surg Infect (Larchmt)* **17**, 385-393 (2016).
30. A. Wang *et al.*, Opposing Effects of Fasting Metabolism on Tissue Tolerance in Bacterial and Viral Inflammation. *Cell* **166**, 1512-1525.e1512 (2016).
31. Y. V. Radzyukevich, N. I. Kosyakova, I. R. Prokhorenko, Participation of Monocyte Subpopulations in Progression of Experimental Endotoxemia (EE) and Systemic Inflammation. *Journal of Immunology Research* **2021**, 1-9 (2021).
32. L. Zhang *et al.*, Splenocyte Apoptosis and Autophagy Is Mediated by Interferon Regulatory Factor 1 During Murine Endotoxemia. *Shock* **37**, 511-517 (2012).

33. E. A. Schwartz *et al.*, Nutrient modification of the innate immune response: a novel mechanism by which saturated fatty acids greatly amplify monocyte inflammation. *Arterioscler Thromb Vasc Biol* **30**, 802-808 (2010).

34. C. Fang *et al.*, Differential regulation of lipopolysaccharide-induced IL-1beta and TNF-alpha production in macrophages by palmitate via modulating TLR4 downstream signaling. *Int Immunopharmacol* **103**, 108456 (2021).

35. S. C. Cheng *et al.*, Broad defects in the energy metabolism of leukocytes underlie immunoparalysis in sepsis. *Nat Immunol* **17**, 406-413 (2016).

36. C. Nedeva, J. Menassa, H. Puthalakath, Sepsis: Inflammation Is a Necessary Evil. *Front Cell Dev Biol* **7**, 108 (2019).

37. C. A. Gogos, E. Drosou, H. P. Bassaris, A. Skoutelis, Pro- versus anti-inflammatory cytokine profile in patients with severe sepsis: a marker for prognosis and future therapeutic options. *J Infect Dis* **181**, 176-180 (2000).

38. J. T. van Dissel, P. van Langevelde, R. G. Westendorp, K. Kwappenberg, M. Frölich, Anti-inflammatory cytokine profile and mortality in febrile patients. *Lancet* **351**, 950-953 (1998).

39. M. De Zuani, J. Frič, Train the Trainer: Hematopoietic Stem Cell Control of Trained Immunity. *Front Immunol* **13**, 827250 (2022).

40. S. E. Vasquez, M. A. Inlay, T. Serwold, CD201 and CD27 identify hematopoietic stem and progenitor cells across multiple murine strains independently of Kit and Sca-1. *Experimental Hematology*, (2015).

41. B. Nowlan, E. D. Williams, M. R. Doran, J.-P. Levesque, CD27, CD201, FLT3, CD48, and CD150 cell surface staining identifies long-term mouse hematopoietic stem cells in immunodeficient non-obese diabetic severe combined immune deficient-derived strains. *Haematologica*, (2020).

42. R. M. Dougherty, C. Galli, A. Ferro-Luzzi, J. M. Iacono, Lipid and phospholipid fatty acid composition of plasma, red blood cells, and platelets and how they are affected by dietary lipids: a study of normal subjects from Italy, Finland, and the USA. *Am J Clin Nutr* **45**, 443-455 (1987).

43. C. M. Skeaff, L. Hodson, J. E. McKenzie, Dietary-induced changes in fatty acid composition of human plasma, platelet, and erythrocyte lipids follow a similar time course. *J Nutr* **136**, 565-569 (2006).

44. N. Zollner, F. Tato, Fatty acid composition of the diet: impact on serum lipids and atherosclerosis. *Clin Investig* **70**, 968-1009 (1992).

45. J. Choi *et al.*, Comprehensive analysis of phospholipids in the brain, heart, kidney, and liver: brain phospholipids are least enriched with polyunsaturated fatty acids. *Mol Cell Biochem* **442**, 187-201 (2018).

46. I. S. S. A, A. B. C, J. S. A, Changes in Plasma Free Fatty Acids Associated with Type-2 Diabetes. *Nutrients* **11**, (2019).

47. E. Sokolowska, A. Blachnio-Zabielska, The Role of Ceramides in Insulin Resistance. *Front Endocrinol (Lausanne)* **10**, 577 (2019).

48. M. Papadimitriou-Olivgeris *et al.*, The Role of Obesity in Sepsis Outcome among Critically Ill Patients: A Retrospective Cohort Analysis. *Biomed Res Int* **2016**, 5941279 (2016).

49. A. Mancini *et al.*, Biological and Nutritional Properties of Palm Oil and Palmitic Acid: Effects on Health. *Molecules* **20**, 17339-17361 (2015).

50. J. Korbecki, K. Bajdak-Rusinek, The effect of palmitic acid on inflammatory response in macrophages: an overview of molecular mechanisms. *Inflamm Res* **68**, 915-932 (2019).

51. S. A. Abdelmagid *et al.*, Comprehensive Profiling of Plasma Fatty Acid Concentrations in Young Healthy Canadian Adults. *PLoS One*, (2015).

52. L. Liu *et al.*, Targeted metabolomic analysis reveals the association between the postprandial change in palmitic acid, branched-chain amino acids and insulin resistance in young obese subjects. *Diabetes Res Clin Pract* **108**, 84-93 (2015).

53. S. F. Gallego, M. Hermansson, G. Liebisch, L. Hodson, C. S. Ejsing, Total Fatty Acid Analysis of Human Blood Samples in One Minute by High-Resolution Mass Spectrometry. *Biomolecules* **9**, (2018).

54. C. D. C. Buchanan *et al.*, Analysis of major fatty acids from matched plasma and serum samples reveals highly comparable absolute and relative levels. *Prostaglandins, Leukotrienes and Essential Fatty Acids* **168**, 102268 (2021).

55. M. Perreault *et al.*, A distinct fatty acid profile underlies the reduced inflammatory state of metabolically healthy obese individuals. *PLoS One* **9**, e88539 (2014).

56. N. M. Borradaile *et al.*, Disruption of endoplasmic reticulum structure and integrity in lipotoxic cell death. *J Lipid Res* **47**, 2726-2737 (2006).

57. H. Li *et al.*, Adipocyte Fatty Acid-Binding Protein Promotes Palmitate-Induced Mitochondrial Dysfunction and Apoptosis in Macrophages. *Front Immunol* **9**, 81 (2018).

58. L. D. Ly *et al.*, Oxidative stress and calcium dysregulation by palmitate in type 2 diabetes. *Exp Mol Med* **49**, e291 (2017).

59. L. Tao *et al.*, RIP1 kinase activity promotes steatohepatitis through mediating cell death and inflammation in macrophages. *Cell Death Differ* **28**, 1418-1433 (2021).

60. X. Palomer, J. Pizarro-Delgado, E. Barroso, M. Vázquez-Carrera, Palmitic and Oleic Acid: The Yin and Yang of Fatty Acids in Type 2 Diabetes Mellitus. *Trends in Endocrinology & Metabolism* **29**, 178-190 (2018).

61. J. Jin *et al.*, Acid sphingomyelinase plays a key role in palmitic acid-amplified inflammatory signaling triggered by lipopolysaccharide at low concentrations in macrophages. *Am J Physiol Endocrinol Metab* **305**, E853-867 (2013).

62. K. Eguchi *et al.*, Saturated fatty acid and TLR signaling link beta cell dysfunction and islet inflammation. *Cell Metab* **15**, 518-533 (2012).

63. D. D. Black, Development and Physiological Regulation of Intestinal Lipid Absorption. I. Development of intestinal lipid absorption: cellular events in chylomicron assembly and secretion. *Am J Physiol Gastrointest Liver Physiol* **293**, (2007).

64. C. M. Mansbach II, F. Gorelick, Development and physiological regulation of intestinal lipid absorption. II. Dietary lipid absorption, complex lipid synthesis, and the intracellular packaging and secretion of chylomicrons. *Am J Physiol Gastrointest Liver Physiol* **293**, (2007).

65. M. H. Karavolos *et al.*, Adrenaline modulates the global transcriptional profile of Salmonella revealing a role in the antimicrobial peptide and oxidative stress resistance responses. *BMC Genomics* **9**, 458 (2008).

66. M. G. Netea *et al.*, Defining trained immunity and its role in health and disease. *Nat Rev Immunol* **20**, 375-388 (2020).

67. L. L. Listenberger *et al.*, Triglyceride accumulation protects against fatty acid-induced lipotoxicity. *Proc Natl Acad Sci U S A* **100**, 3077-3082 (2003).

68. S. Bekkering *et al.*, Oxidized low-density lipoprotein induces long-term proinflammatory cytokine production and foam cell formation via epigenetic reprogramming of monocytes. *Arterioscler Thromb Vasc Biol* **34**, 1731-1738 (2014).

69. T. S. Ayala *et al.*, High glucose environments interfere with bone marrow-derived macrophage inflammatory mediator release, the TLR4 pathway and glucose metabolism. *Scientific Reports*, (2019).

70. P. Y. Ng, M. Eikermann, The obesity conundrum in sepsis. *BMC Anesthesiol* **17**, 147 (2017).

71. K. D. Hall, S. T. Chung, Effect of a plant-based, low-fat diet versus an animal-based, ketogenic diet on ad libitum energy intake. *Nature Medicine*, (2021).

72. A. R. Kennedy, E. Maratos-Flier, A high-fat, ketogenic diet induces a unique metabolic state in mice. *The American Journal of Physiology - Endocrinology and Metabolism*, (2007).

73. S. Galadari, A. Rahman, S. Pallichankandy, A. Galadari, F. Thayyullathil, Role of ceramide in diabetes mellitus: evidence and mechanisms. *Lipids Health Dis* **12**, 98 (2013).

74. A. R. DiNardo, M. G. Netea, D. M. Musher, Postinfectious Epigenetic Immune Modifications - A Double-Edged Sword. *N Engl J Med* **384**, 261-270 (2021).

75. B. Beutler, I. W. Milsark, A. C. Cerami, Passive immunization against cachectin/tumor necrosis factor protects mice from lethal effect of endotoxin. *Science* **229**, 869-871 (1985).

76. K. M. Mohler *et al.*, Soluble tumor necrosis factor (TNF) receptors are effective therapeutic agents in lethal endotoxemia and function simultaneously as both TNF carriers and TNF antagonists. *J Immunol* **151**, 1548-1561 (1993).

77. P. N. Cunningham *et al.*, Acute renal failure in endotoxemia is caused by TNF acting directly on TNF receptor-1 in kidney. *J Immunol* **168**, 5817-5823 (2002).

78. Y. Chen *et al.*, Aerosol synthesis of cargo-filled graphene nanosacks. *Nano Lett* **12**, 1996-2002 (2012).

79. W. Zhong *et al.*, Curcumin alleviates lipopolysaccharide induced sepsis and liver failure by suppression of oxidative stress-related inflammation via PI3K/AKT and NF-κB related signaling. *Biomed Pharmacother* **83**, 302-313 (2016).

80. L. E. Escobar, A. Molina-Cruz, C. Barillas-Mury, BCG vaccine protection from severe coronavirus disease 2019 (COVID-19). *Proc Natl Acad Sci U S A* **117**, 17720-17726 (2020).

81. R. J. Arts *et al.*, Glutaminolysis and Fumarate Accumulation Integrate Immunometabolic and Epigenetic Programs in Trained Immunity. *Cell Metab* **24**, 807-819 (2016).

82. D. G. Ryan, L. A. J. O'Neill, Krebs Cycle Reborn in Macrophage Immunometabolism. *Annu Rev Immunol* **38**, 289-313 (2020).

83. G. D. Silva, F. C. Brochers-Lacchini, A. M. Leopoldino, How do sphingolipids play a role in epigenetic mechanisms and gene expression? *Epigenomics*, (2021).

84. D. G. Souza *et al.*, The essential role of the intestinal microbiota in facilitating acute inflammatory responses. *J Immunol* **173**, 4137-4146 (2004).

85. A. K. F. Mundt *et al.* (2017).

86. Wickham *et al.* (Springer International Publishing, 2016).

87. Lê *et al.*, FactoMineR:an R package for multivariate analysis. *J.Stat. Soft* (2008).

88. Kolde *et al.* (2018).

Figure 1

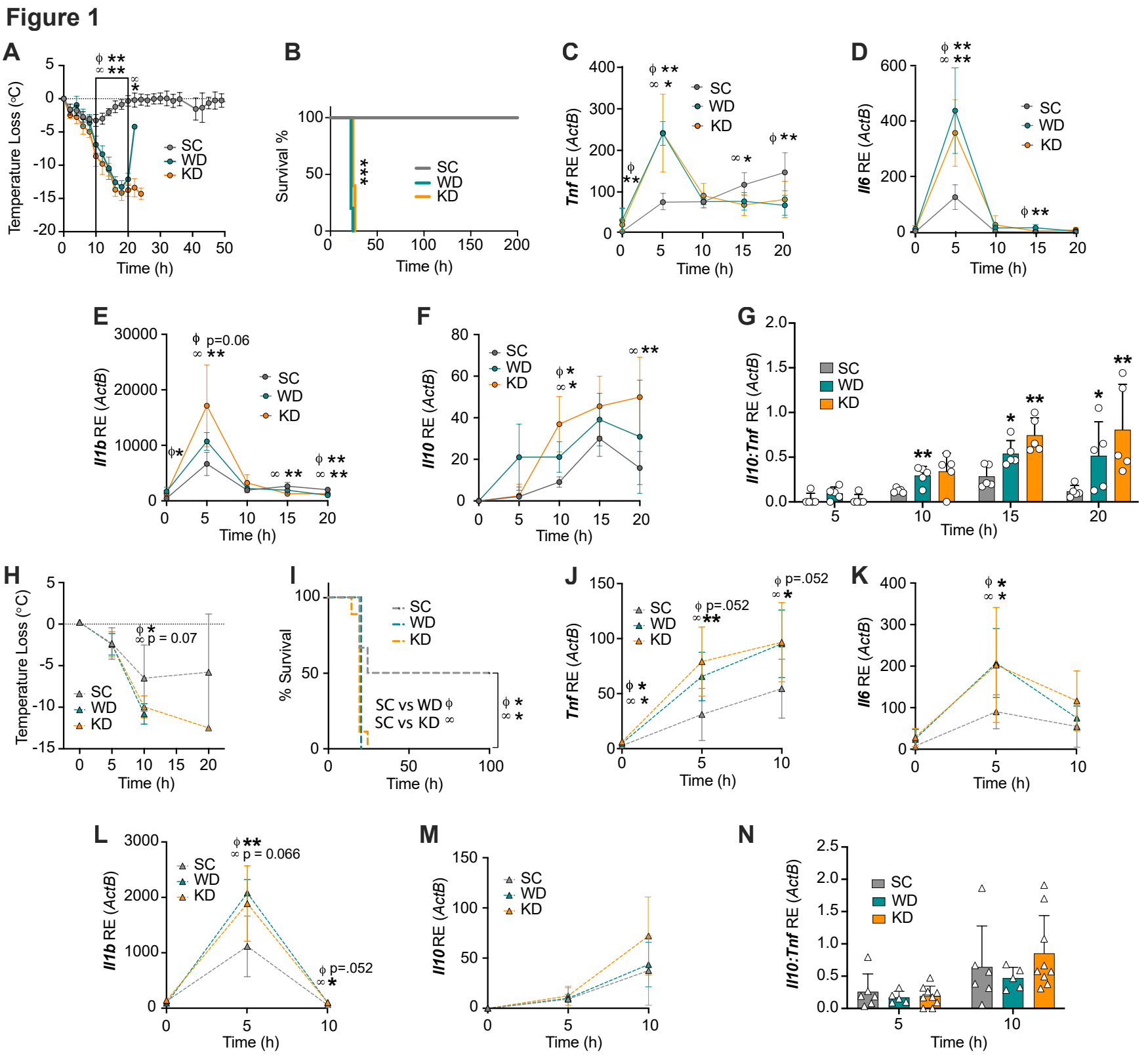
A
Temperature Loss (°C)
Time (h)
SC
WD
KD
B
Survival %
Time (h)
C
Tnf RE (ActB)
D
Il6 RE (ActB)
E
Il1b RE (ActB)
p=0.06
F
Il10 RE (ActB)
G
Il10:Tnf RE (ActB)
H
p = 0.07
I
% Survival
SC vs WD ϕ
SC vs KD ∞
J
p=.052
K
L
p = 0.066
M
N

Figure 2

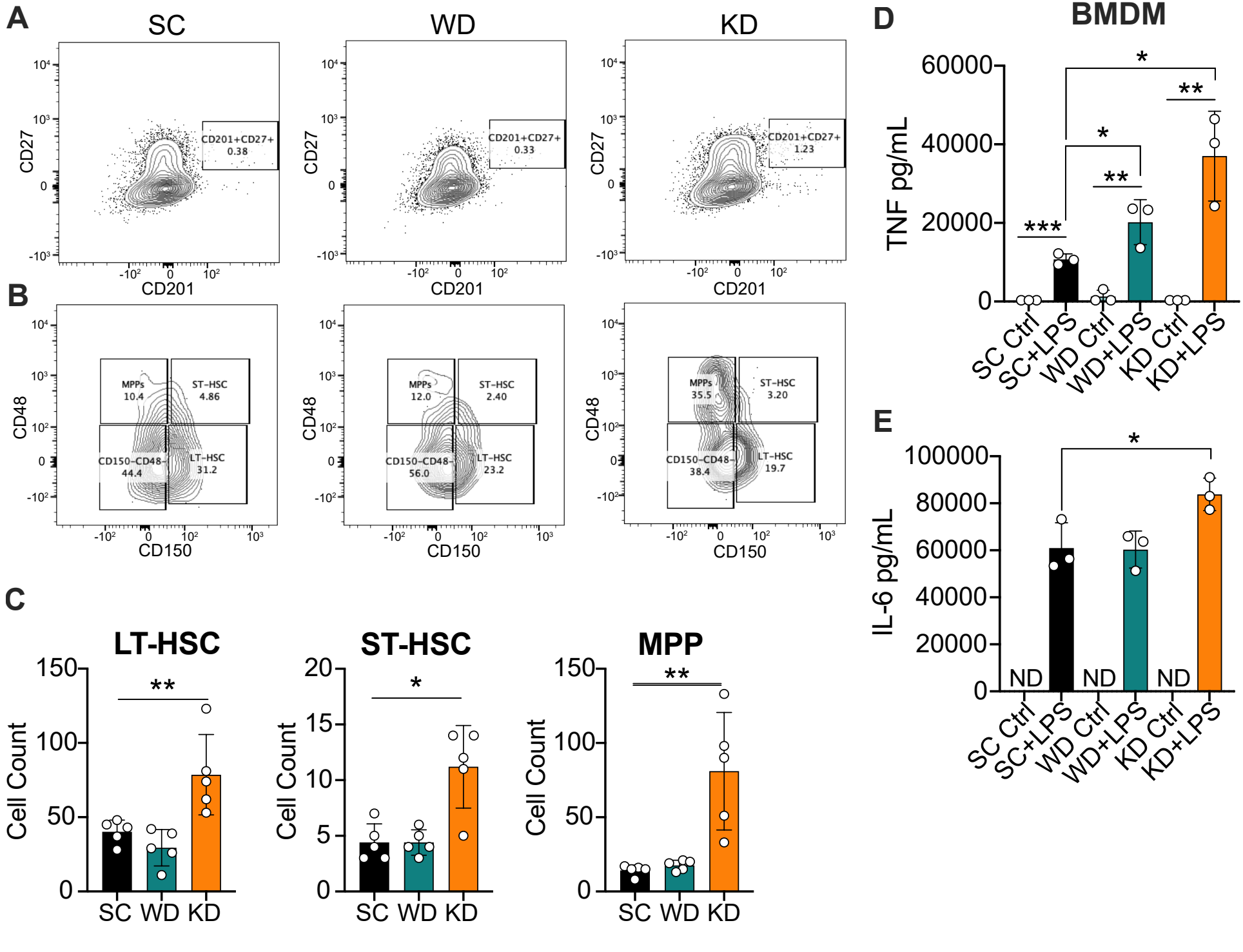
A
SC
WD
KD
CD27
CD201
CD201+CD27+
0.38
0.33
1.23
B
CD48
CD150
MPPs
10.4
12.0
35.5
ST-HSC
4.86
2.40
3.20
CD150-CD48-
44.4
56.0
38.4
LT-HSC
31.2
23.2
19.7
C
LT-HSC
ST-HSC
MPP
Cell Count
SC WD KD
D
BMDM
TNF pg/mL
SC Ctrl
SC+LPS
WD Ctrl
WD+LPS
KD Ctrl
KD+LPS
E
IL-6 pg/mL
ND

Figure 3

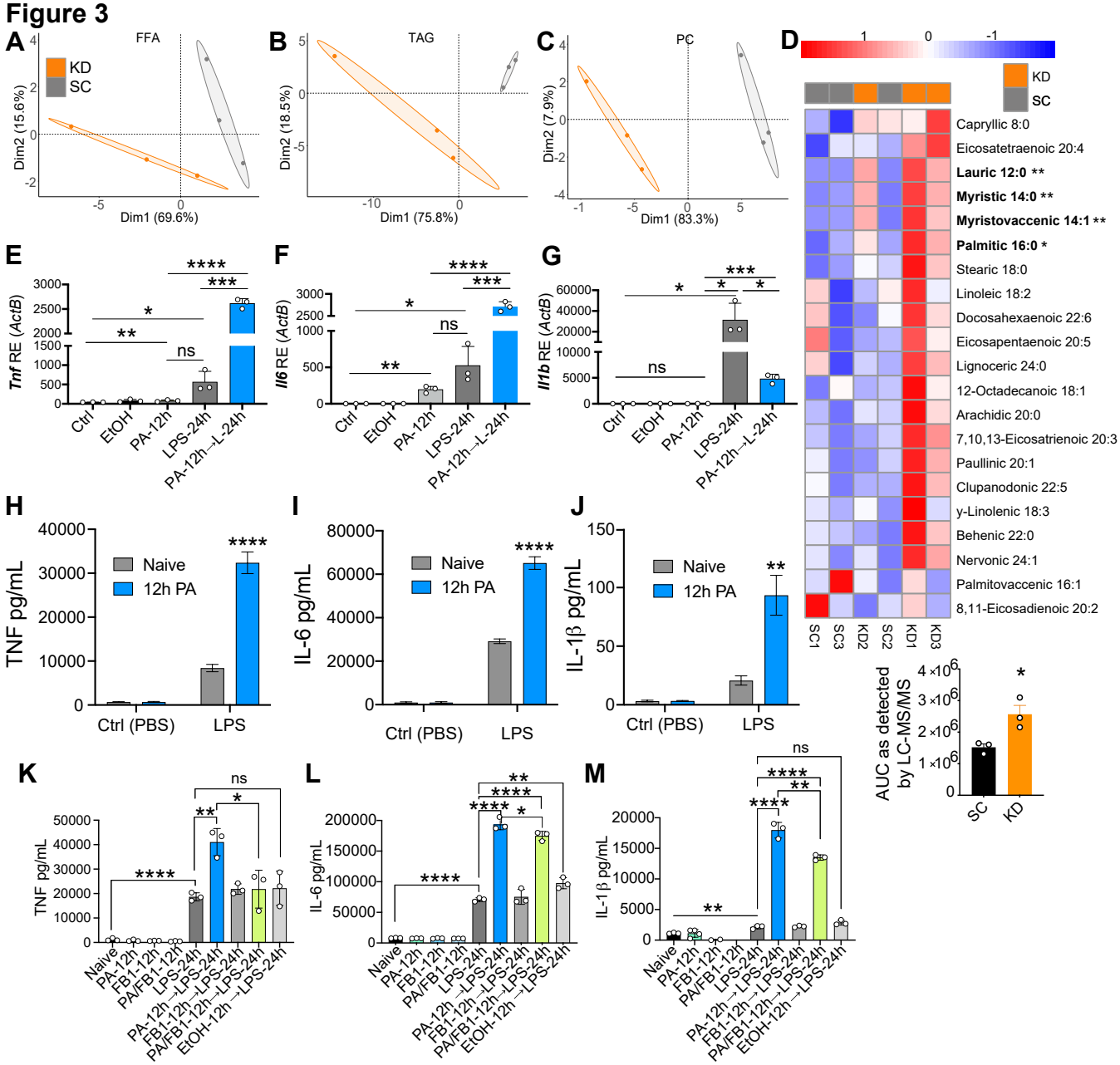
A
FFA
KD
SC
Dim2 (15.6%)
Dim1 (69.6%)
B
TAG
Dim2 (18.5%)
Dim1 (75.8%)
C
PC
Dim2 (7.9%)
Dim1 (83.3%)
D
1
0
-1
KD
SC
Capryllic 8:0
Eicosatetraenoic 20:4
Lauric 12:0 **
Myristic 14:0 **
Myristovaccenic 14:1 **
Palmitic 16:0 *
Stearic 18:0
Linoleic 18:2
Docosahexaenoic 22:6
Eicosapentaenoic 20:5
Lignoceric 24:0
12-Octadecanoic 18:1
Arachidic 20:0
7,10,13-Eicosatrienoic 20:3
Paullinic 20:1
Clupanodonic 22:5
y-Linolenic 18:3
Behenic 22:0
Nervonic 24:1
Palmitovaccenic 16:1
8,11-Eicosadienoic 20:2
SC1
SC3
KD2
SC2
KD1
KD3
E
Tnf RE (ActB)
F
Il6 RE (ActB)
G
Il1b RE (ActB)
Ctrl
EtOH
PA-12h
LPS-24h
PA-12h→L-24h
H
TNF pg/mL
Naive
12h PA
Ctrl (PBS)
LPS
I
IL-6 pg/mL
J
IL-1β pg/mL
AUC as detected by LC-MS/MS
SC
KD
K
TNF pg/mL
L
IL-6 pg/mL
M
IL-1 β pg/mL
Naive
PA-12h
FB1-12h
PA/FB1-12h
LPS-24h
PA-12h→LPS-24h
FB1-12h→LPS-24h
PA/FB1-12h→LPS-24h
EtOH-12h→LPS-24h

Figure 4

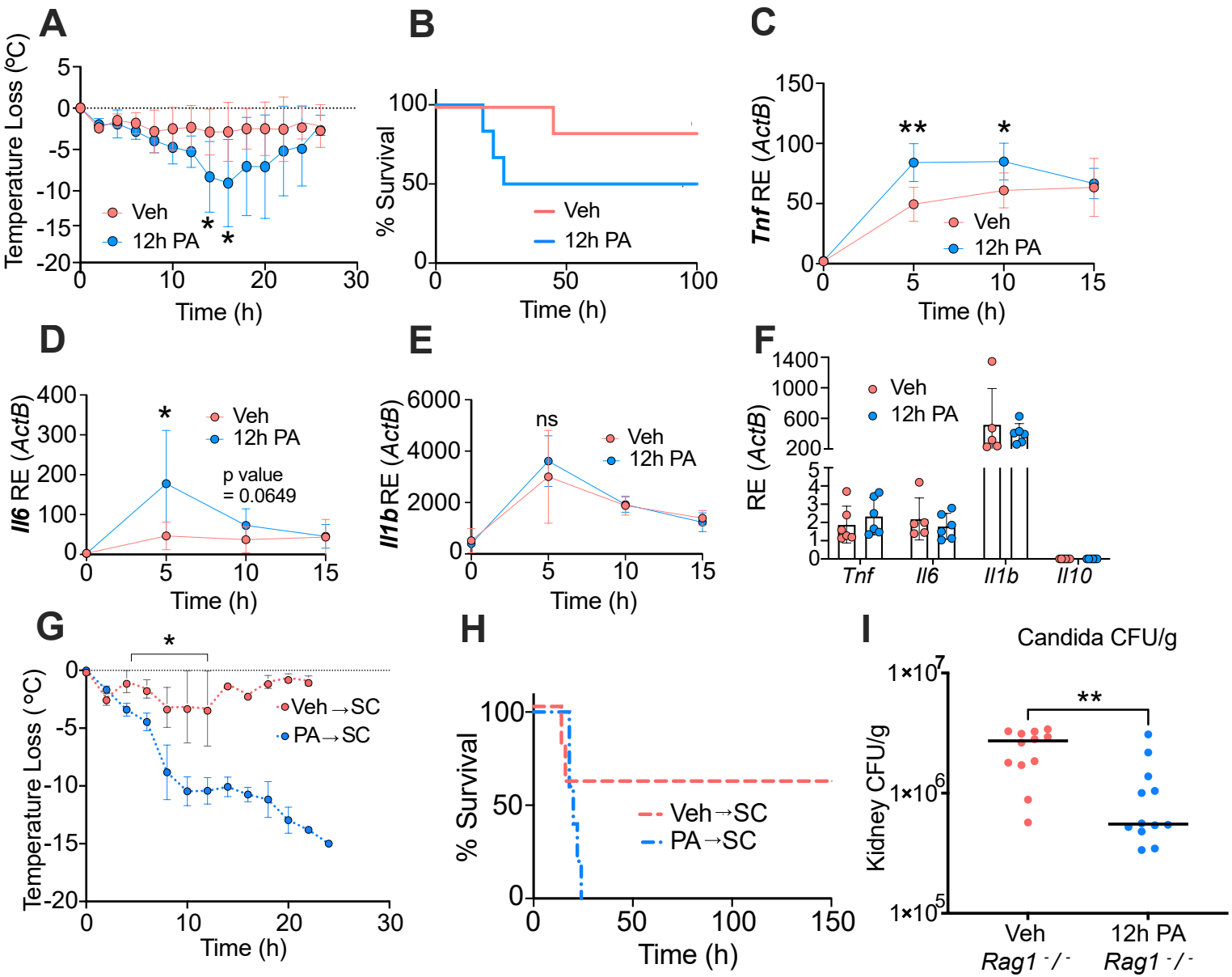
A
Temperature Loss (ºC)
Time (h)
Veh
12h PA
B
% Survival
Time (h)
Veh
12h PA
C
Tnf RE (ActB)
Time (h)
Veh
12h PA
D
Il6 RE (ActB)
Time (h)
Veh
12h PA
p value
= 0.0649
E
Il1b RE (ActB)
Time (h)
ns
Veh
12h PA
F
RE (ActB)
Veh
12h PA
Tnf
Il6
Il1b
Il10
G
Temperature Loss (ºC)
Time (h)
Veh→SC
PA→SC
H
% Survival
Time (h)
Veh→SC
PA→SC
I
Candida CFU/g
Kidney CFU/g
Veh
Rag1 -/-
12h PA
Rag1 -/-

Figure 5

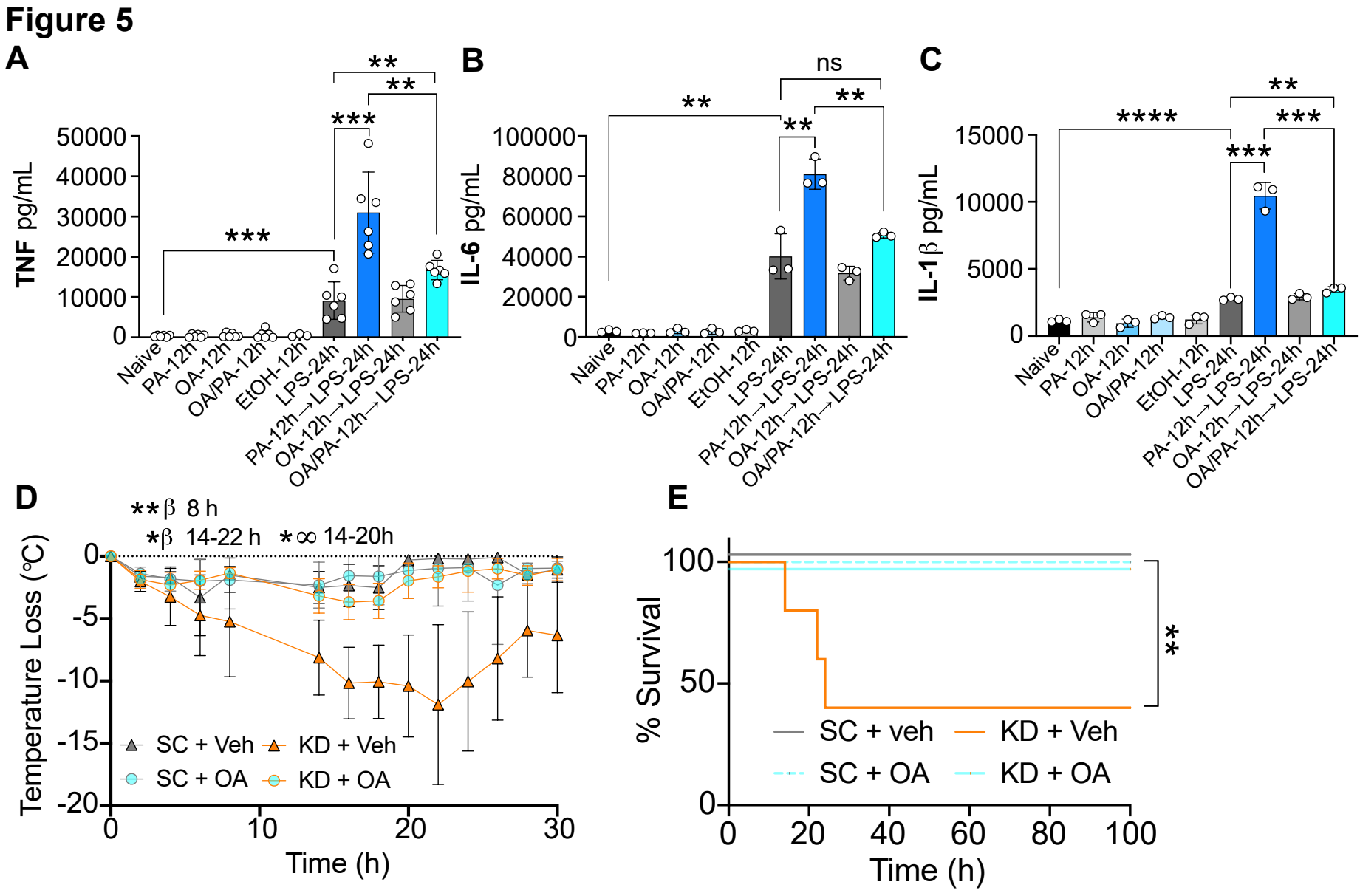
A
TNF pg/mL
50000
40000
30000
20000
10000
0
***
**
**
***
Naive
PA-12h
OA-12h
OA/PA-12h
EtOH-12h
LPS-24h
PA-12h→LPS-24h
OA-12h→LPS-24h
OA/PA-12h→LPS-24h
B
IL-6 pg/mL
100000
80000
60000
40000
20000
0
**
ns
**
**
C
IL-1β pg/mL
15000
10000
5000
0
****
***
**
***
D
**β 8 h
*β 14-22 h *∞ 14-20h
Temperature Loss (°C)
0
-5
-10
-15
-20
SC + Veh
KD + Veh
SC + OA
KD + OA
0
10
20
30
Time (h)
E
% Survival
100
50
0
SC + veh
KD + Veh
SC + OA
KD + OA
**
0
20
40
60
80
100
Time (h)

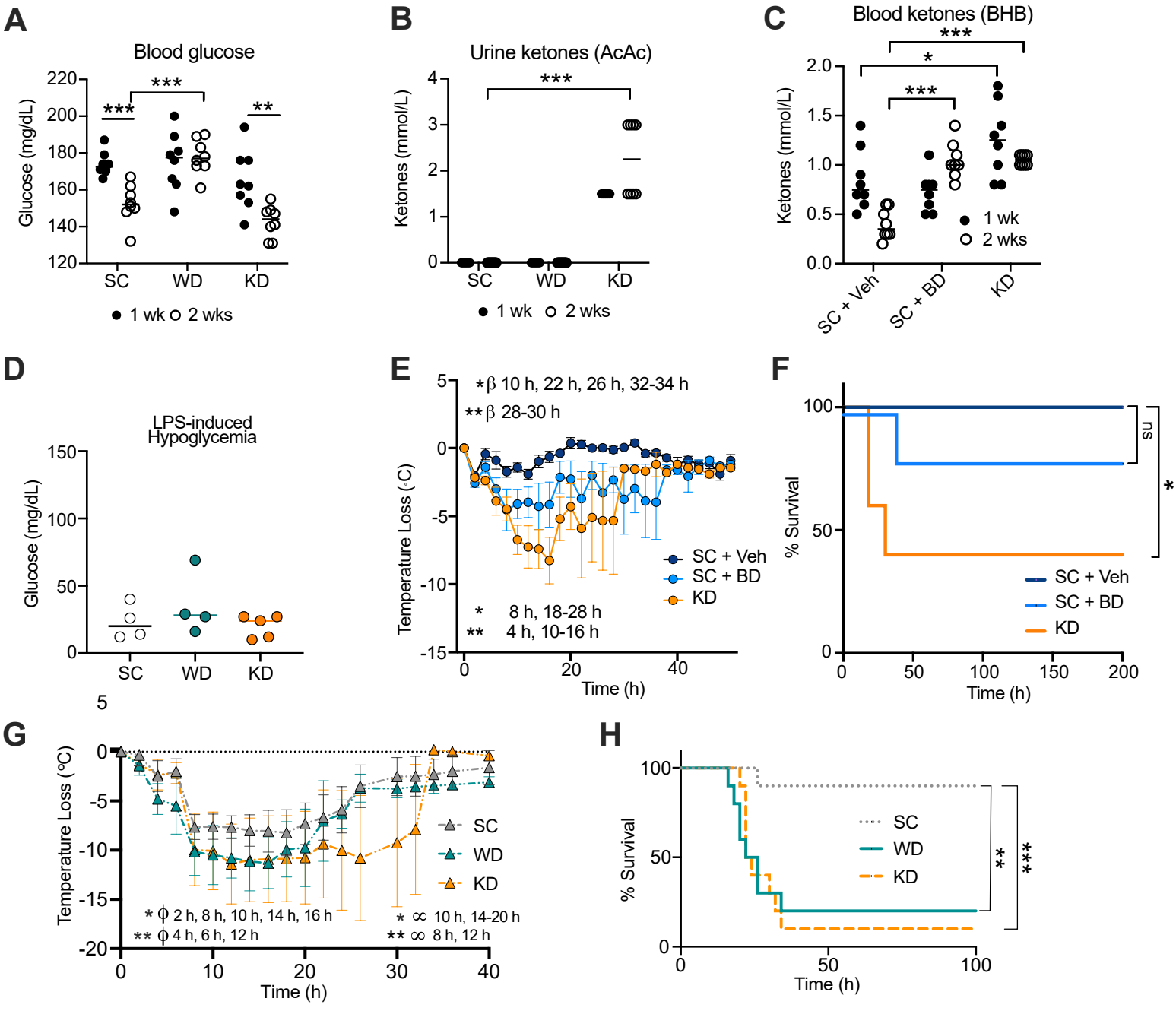
A
Blood glucose
Glucose (mg/dL)
220
200
180
160
140
120
***
***
**
SC
WD
KD
1 wk
2 wks
B
Urine ketones (AcAc)
Ketones (mmol/L)
4
3
2
1
0
***
SC
WD
KD
1 wk
2 wks
C
Blood ketones (BHB)
***
*
***
Ketones (mmol/L)
2.0
1.5
1.0
0.5
0.0
1 wk
2 wks
SC + Veh
SC + BD
KD
D
LPS-induced
Hypoglycemia
Glucose (mg/dL)
150
100
50
0
SC
WD
KD
5
E
*β 10 h, 22 h, 26 h, 32-34 h
**β 28-30 h
Temperature Loss (°C)
5
0
-5
-10
-15
SC + Veh
SC + BD
KD
* 8 h, 18-28 h
** 4 h, 10-16 h
0
20
40
Time (h)
F
% Survival
100
50
0
ns
*
SC + Veh
SC + BD
KD
0
50
100
150
200
Time (h)
G
Temperature Loss (°C)
0
-5
-10
-15
-20
SC
WD
KD
* ϕ 2 h, 8 h, 10 h, 14 h, 16 h
** ϕ 4 h, 6 h, 12 h
* ∞ 10 h, 14-20 h
** ∞ 8 h, 12 h
0
10
20
30
40
Time (h)
H
% Survival
100
50
0
SC
WD
KD
**
***
0
50
100
Time (h)

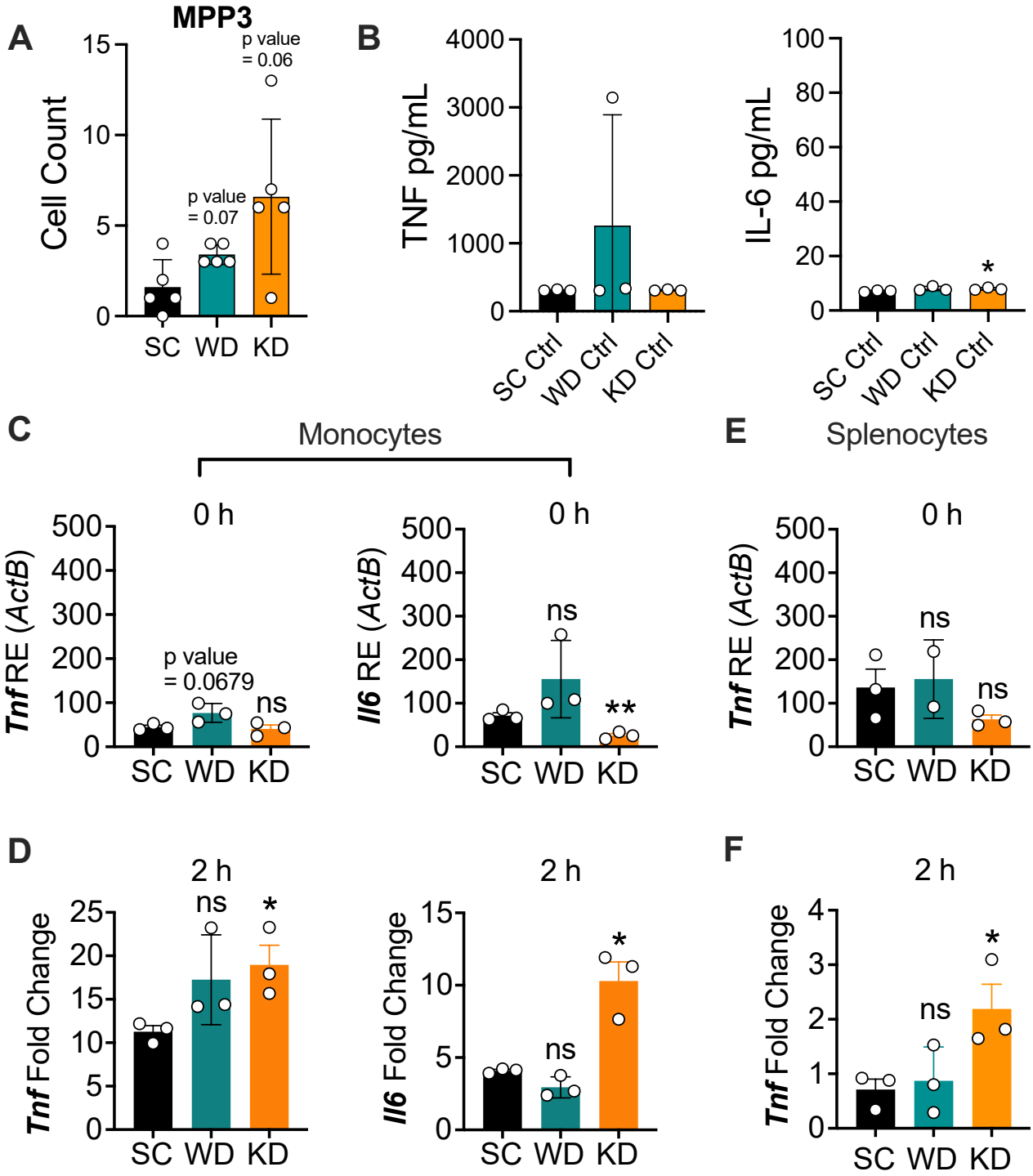
A
MPP3
Cell Count
p value = 0.06
p value = 0.07
SC WD KD
B
TNF pg/mL
SC Ctrl
WD Ctrl
KD Ctrl
IL-6 pg/mL
*
C
Monocytes
0 h
Tnf RE (ActB)
p value = 0.0679
ns
Il6 RE (ActB)
**
D
2 h
Tnf Fold Change
Il6 Fold Change
E
Splenocytes
F

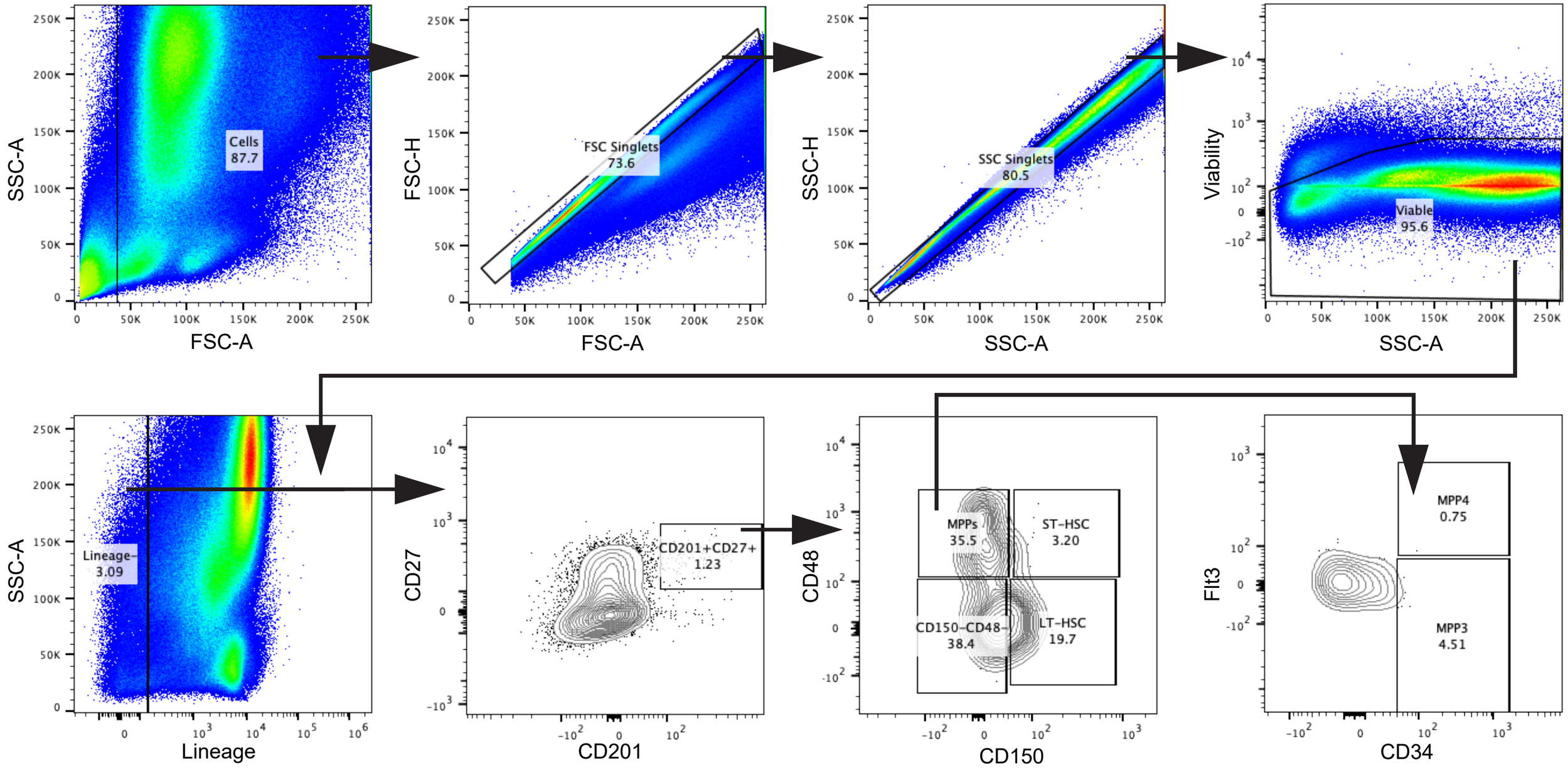
SSC-A
FSC-A
Cells
87.7
FSC-H
FSC-A
FSC Singlets
73.6
SSC-H
SSC-A
SSC Singlets
80.5
Viability
SSC-A
Viable
95.6
SSC-A
Lineage
Lineage-
3.09
CD27
CD201
CD201+CD27+
1.23
CD48
CD150
MPPs
35.5
ST-HSC
3.20
CD150-CD48-
38.4
LT-HSC
19.7
Flt3
CD34
MPP4
0.75
MPP3
4.51

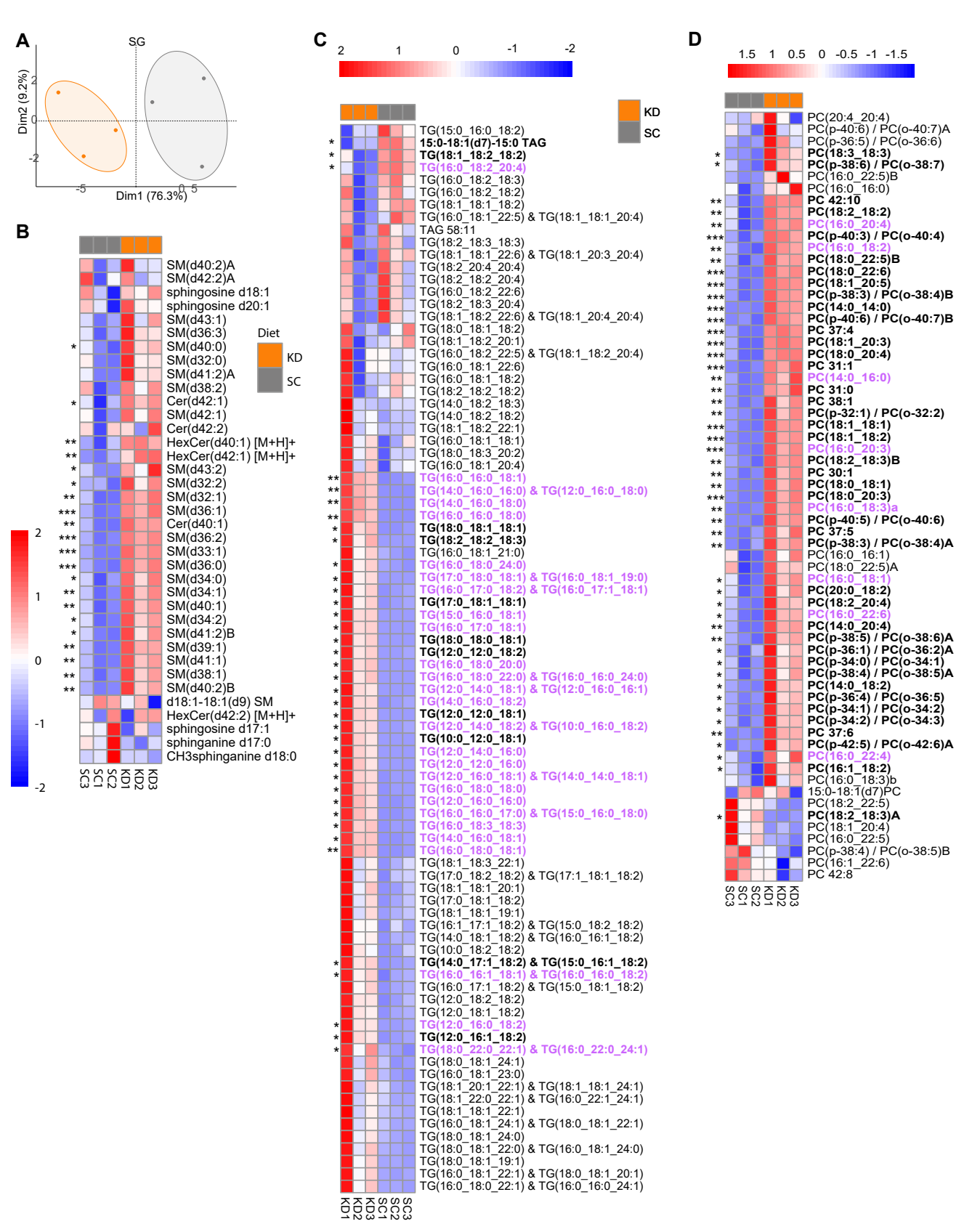
A
SG
Dim2 (9.2%)
Dim1 (76.3%)
B
Diet
KD
SC
SM(d40:2)A
SM(d42:2)A
sphingosine d18:1
sphingosine d20:1
SM(d43:1)
SM(d36:3)
SM(d40:0)
SM(d32:0)
SM(d41:2)A
SM(d38:2)
Cer(d42:1)
SM(d42:1)
Cer(d42:2)
HexCer(d40:1) [M+H]+
HexCer(d42:1) [M+H]+
SM(d43:2)
SM(d32:2)
SM(d32:1)
SM(d36:1)
Cer(d40:1)
SM(d36:2)
SM(d33:1)
SM(d36:0)
SM(d34:0)
SM(d34:1)
SM(d40:1)
SM(d34:2)
SM(d41:2)B
SM(d39:1)
SM(d41:1)
SM(d38:1)
SM(d40:2)B
d18:1-18:1(d9) SM
HexCer(d42:2) [M+H]+
sphingosine d17:1
sphinganine d17:0
CH3sphinganine d18:0
SC3 SC1 SC2 KD1 KD2 KD3
C
KD
SC
TG(15:0_16:0_18:2)
15:0-18:1(d7)-15:0 TAG
TG(18:1_18:2_18:2)
TG(16:0_18:2_20:4)
TG(16:0_18:2_18:3)
TG(16:0_18:2_18:2)
TG(18:1_18:1_18:2)
TG(16:0_18:1_22:5) & TG(18:1_18:1_20:4)
TAG 58:11
TG(18:2_18:3_18:3)
TG(18:1_18:1_22:6) & TG(18:1_20:3_20:4)
TG(18:2_20:4_20:4)
TG(18:2_18:2_20:4)
TG(16:0_18:2_22:6)
TG(18:2_18:3_20:4)
TG(18:1_18:2_22:6) & TG(18:1_20:4_20:4)
TG(18:0_18:1_18:2)
TG(18:1_18:2_20:1)
TG(16:0_18:2_22:5) & TG(18:1_18:2_20:4)
TG(16:0_18:1_22:6)
TG(16:0_18:1_18:2)
TG(18:2_18:2_18:2)
TG(14:0_18:2_18:3)
TG(14:0_18:2_18:2)
TG(18:1_18:2_22:1)
TG(16:0_18:1_18:1)
TG(18:0_18:3_20:2)
TG(16:0_18:1_20:4)
TG(16:0_16:0_18:1)
TG(14:0_16:0_16:0) & TG(12:0_16:0_18:0)
TG(14:0_16:0_18:0)
TG(16:0_16:0_18:0)
TG(18:0_18:1_18:1)
TG(18:2_18:2_18:3)
TG(16:0_18:1_21:0)
TG(16:0_18:0_24:0)
TG(17:0_18:0_18:1) & TG(16:0_18:1_19:0)
TG(16:0_17:0_18:2) & TG(16:0_17:1_18:1)
TG(17:0_18:1_18:1)
TG(15:0_16:0_18:1)
TG(16:0_17:0_18:1)
TG(18:0_18:0_18:1)
TG(12:0_12:0_18:2)
TG(16:0_18:0_20:0)
TG(16:0_18:0_22:0) & TG(16:0_16:0_24:0)
TG(12:0_14:0_18:1) & TG(12:0_16:0_16:1)
TG(14:0_16:0_18:2)
TG(12:0_12:0_18:1)
TG(12:0_14:0_18:2) & TG(10:0_16:0_18:2)
TG(10:0_12:0_18:1)
TG(12:0_14:0_16:0)
TG(12:0_12:0_16:0)
TG(12:0_16:0_18:1) & TG(14:0_14:0_18:1)
TG(16:0_18:0_18:0)
TG(12:0_16:0_16:0)
TG(16:0_16:0_17:0) & TG(15:0_16:0_18:0)
TG(16:0_18:3_18:3)
TG(14:0_16:0_18:1)
TG(16:0_18:0_18:1)
TG(18:1_18:3_22:1)
TG(17:0_18:2_18:2) & TG(17:1_18:1_18:2)
TG(18:1_18:1_20:1)
TG(17:0_18:1_18:2)
TG(18:1_18:1_19:1)
TG(16:1_17:1_18:2) & TG(15:0_18:2_18:2)
TG(14:0_18:1_18:2) & TG(16:0_16:1_18:2)
TG(10:0_18:2_18:2)
TG(14:0_17:1_18:2) & TG(15:0_16:1_18:2)
TG(16:0_16:1_18:1) & TG(16:0_16:0_18:2)
TG(16:0_17:1_18:2) & TG(15:0_18:1_18:2)
TG(12:0_18:2_18:2)
TG(12:0_18:1_18:2)
TG(12:0_16:0_18:2)
TG(12:0_16:1_18:2)
TG(18:0_22:0_22:1) & TG(16:0_22:0_24:1)
TG(18:0_18:1_24:1)
TG(16:0_18:1_23:0)
TG(18:1_20:1_22:1) & TG(18:1_18:1_24:1)
TG(18:1_22:0_22:1) & TG(16:0_22:1_24:1)
TG(18:1_18:1_22:1)
TG(16:0_18:1_24:1) & TG(18:0_18:1_22:1)
TG(18:0_18:1_24:0)
TG(18:0_18:1_22:0) & TG(16:0_18:1_24:0)
TG(18:0_18:1_19:1)
TG(16:0_18:1_22:1) & TG(18:0_18:1_20:1)
TG(16:0_18:0_22:1) & TG(16:0_16:0_24:1)
KD1 KD2 KD3 SC1 SC2 SC3
D
PC(20:4_20:4)
PC(p-40:6) / PC(o-40:7)A
PC(p-36:5) / PC(o-36:6)
PC(18:3_18:3)
PC(p-38:6) / PC(o-38:7)
PC(16:0_22:5)B
PC(16:0_16:0)
PC 42:10
PC(18:2_18:2)
PC(16:0_20:4)
PC(p-40:3) / PC(o-40:4)
PC(16:0_18:2)
PC(18:0_22:5)B
PC(18:0_22:6)
PC(18:1_20:5)
PC(p-38:3) / PC(o-38:4)B
PC(14:0_14:0)
PC(p-40:6) / PC(o-40:7)B
PC 37:4
PC(18:1_20:3)
PC(18:0_20:4)
PC 31:1
PC(14:0_16:0)
PC 31:0
PC 38:1
PC(p-32:1) / PC(o-32:2)
PC(18:1_18:1)
PC(18:1_18:2)
PC(16:0_20:3)
PC(18:2_18:3)B
PC 30:1
PC(18:0_18:1)
PC(18:0_20:3)
PC(16:0_18:3)a
PC(p-40:5) / PC(o-40:6)
PC 37:5
PC(p-38:3) / PC(o-38:4)A
PC(16:0_16:1)
PC(18:0_22:5)A
PC(16:0_18:1)
PC(20:0_18:2)
PC(18:2_20:4)
PC(16:0_22:6)
PC(14:0_20:4)
PC(p-38:5) / PC(o-38:6)A
PC(p-36:1) / PC(o-36:2)A
PC(p-34:0) / PC(o-34:1)
PC(p-38:4) / PC(o-38:5)A
PC(14:0_18:2)
PC(p-36:4) / PC(o-36:5)
PC(p-34:1) / PC(o-34:2)
PC(p-34:2) / PC(o-34:3)
PC 37:6
PC(p-42:5) / PC(o-42:6)A
PC(16:0_22:4)
PC(16:1_18:2)
PC(16:0_18:3)b
15:0-18:1(d7)PC
PC(18:2_22:5)
PC(18:2_18:3)A
PC(18:1_20:4)
PC(16:0_22:5)
PC(p-38:4) / PC(o-38:5)B
PC(16:1_22:6)
PC 42:8
SC3 SC1 SC2 KD1 KD2 KD3

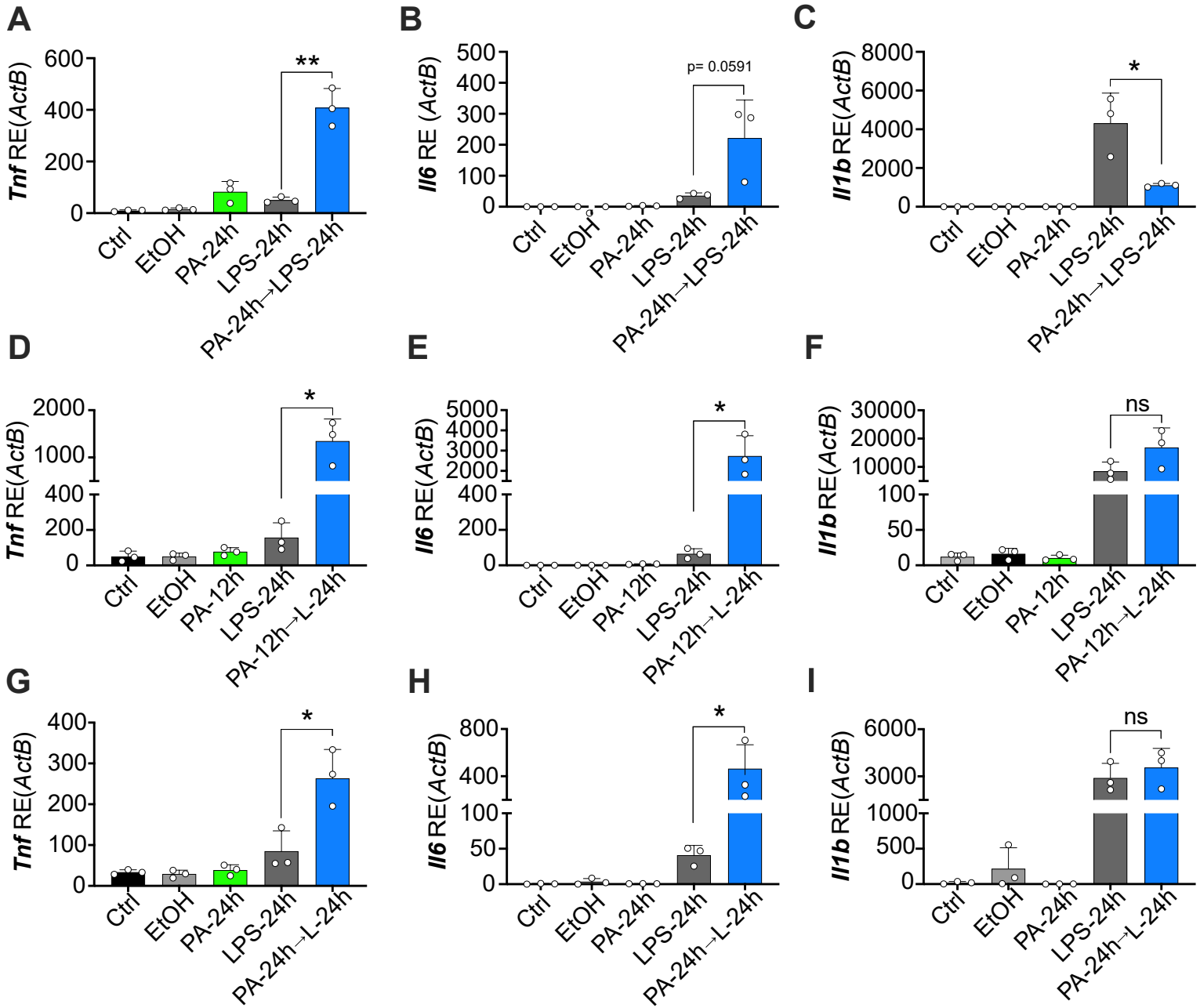
A
Tnf RE(ActB)
600
400
200
0
**
Ctrl
EtOH
PA-24h
LPS-24h
PA-24h→LPS-24h
B
Il6 RE (ActB)
500
400
300
200
100
0
p= 0.0591
Ctrl
EtOH
PA-24h
LPS-24h
PA-24h→LPS-24h
C
Il1b RE(ActB)
8000
6000
4000
2000
0
*
Ctrl
EtOH
PA-24h
LPS-24h
PA-24h→LPS-24h
D
Tnf RE(ActB)
2000
1000
400
200
0
*
Ctrl
EtOH
PA-12h
LPS-24h
PA-12h→L-24h
E
Il6 RE(ActB)
5000
4000
3000
2000
400
200
0
*
Ctrl
EtOH
PA-12h
LPS-24h
PA-12h→L-24h
F
Il1b RE(ActB)
30000
20000
10000
100
50
0
ns
Ctrl
EtOH
PA-12h
LPS-24h
PA-12h→L-24h
G
Tnf RE(ActB)
400
300
200
100
0
*
Ctrl
EtOH
PA-24h
LPS-24h
PA-24h→L-24h
H
Il6 RE(ActB)
800
400
100
50
0
*
Ctrl
EtOH
PA-24h
LPS-24h
PA-24h→L-24h
I
Il1b RE(ActB)
6000
3000
1000
500
0
ns
Ctrl
EtOH
PA-24h
LPS-24h
PA-24h→L-24h

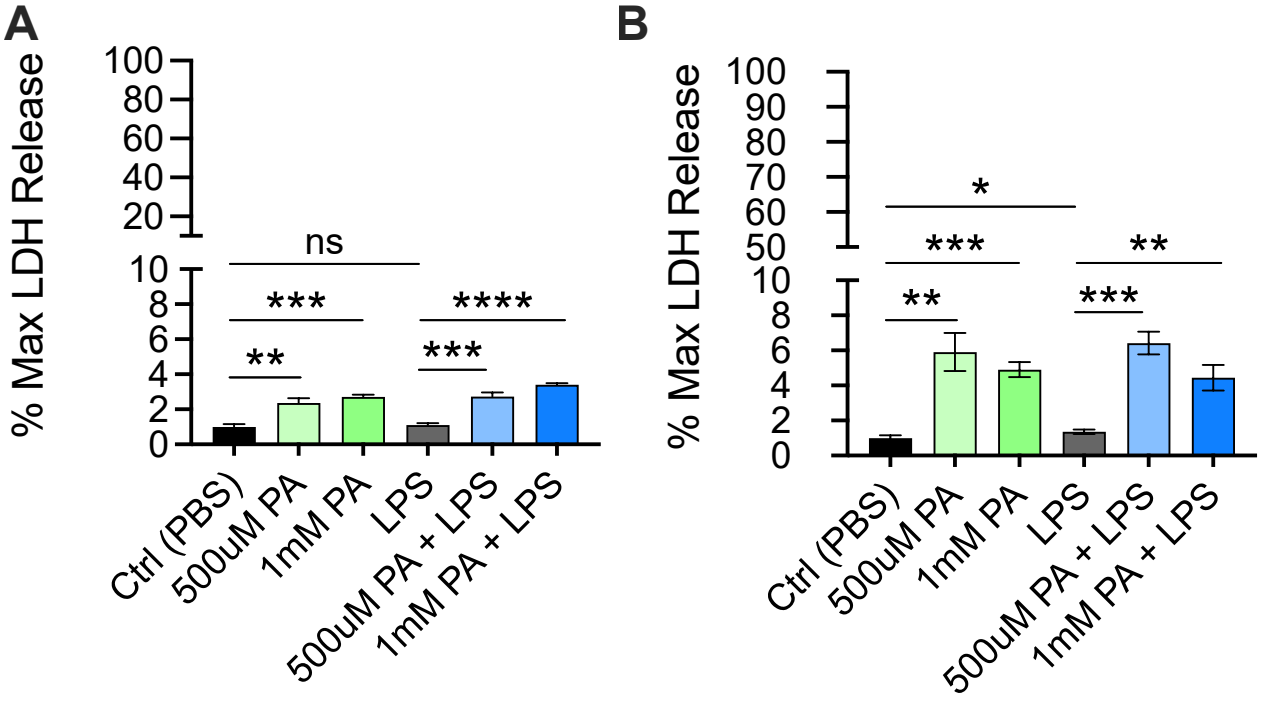
A
% Max LDH Release
100
80
60
40
20
10
8
6
4
2
0
ns
***
**
****
***
Ctrl (PBS)
500uM PA
1mM PA
LPS
500uM PA + LPS
1mM PA + LPS
B
% Max LDH Release
100
90
80
70
60
50
10
8
6
4
2
0
*
***
**
**
***
Ctrl (PBS)
500uM PA
1mM PA
LPS
500uM PA + LPS
1mM PA + LPS

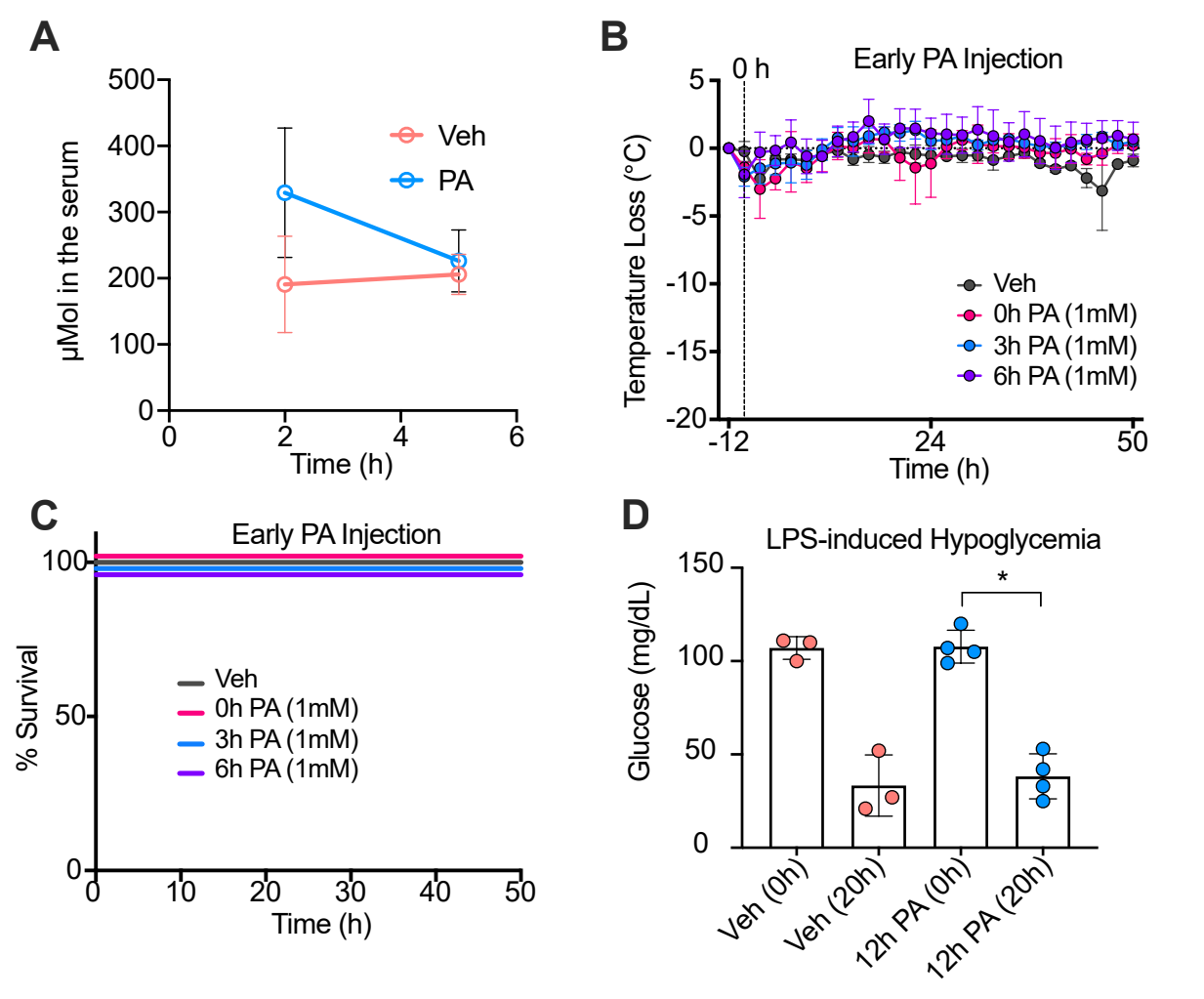
A
500
400
300
200
100
0
µMol in the serum
Veh
PA
0
2
4
6
Time (h)
B
0 h
Early PA Injection
5
0
-5
-10
-15
-20
Temperature Loss (°C)
Veh
0h PA (1mM)
3h PA (1mM)
6h PA (1mM)
-12
24
50
Time (h)
C
Early PA Injection
100
50
0
% Survival
Veh
0h PA (1mM)
3h PA (1mM)
6h PA (1mM)
0
10
20
30
40
50
Time (h)
D
LPS-induced Hypoglycemia
150
100
50
0
Glucose (mg/dL)
*
Veh (0h)
Veh (20h)
12h PA (0h)
12h PA (20h)